Single Cell Analysis Reveals Immune Cell-Adipocyte Crosstalk Regulating the Transcription of Thermogenic Adipocytes

Prashant Rajbhandari[1*], Douglas Arneson[4,5*], An-Chieh Feng[6], In Sook Ahn[4], Graciel Diamante[4,5], Nima Zaghari[5], Brandon J. Thomas[6], Laurent Vergnes[7], Stephen D. Lee[1], Karen Reue[3,7], Stephen T. Smale[3,5], Xia Yang[3,4,5,8] and Peter Tontonoz[1,2,3,8,9]

[1]Department of Pathology and Laboratory Medicine,
[2]Departmemt of Biological Chemistry
[3]Molecular Biology Institute,
[4]Department of Integrative Biology and Physiology,
[5]Bioinformatics Interdepartmental Program,
[6]Department of Microbiology, Immunology, and Molecular Genetics,
[7]Department of Human Genetics,
David Geffen School of Medicine, University of California, Los Angeles, California 90095, USA

[8]Senior Author

[9]Lead Contact

[*]Equal first authors

Corresponding authors:

Peter Tontonoz MD PhD (Lead contact)
Department of Pathology and Laboratory Medicine
University of California, Los Angeles
675 Charles Young Dr., MRL 6-770
Los Angeles, CA 90095-1732 USA
Office (310) 206-4546
E-mail: ptontonoz@mednet.ucla.edu

Prashant Rajbhandari PhD
Department of Pathology and Laboratory Medicine
University of California, Los Angeles
675 Charles Young Dr., MRL 6-619
Los Angeles, CA 90095-1732 USA
Office (310) 206-4622
E-mail: prajbhandari@ucla.edu

Summary

Immune cells are vital constituents of the adipose microenvironment that influence both local and systemic lipid metabolism. Mice lacking IL10 have enhanced thermogenesis, but the roles of specific cell types in the metabolic response to IL10 remain to be defined. We demonstrate here that selective loss of IL10 receptor α in adipocytes recapitulates the beneficial effects of global IL10 deletion, and that local crosstalk between IL10-producing immune cells and adipocytes is a determinant of thermogenesis and systemic energy balance. Single Nuclei Adipocyte RNA-sequencing (SNAP-seq) of subcutaneous adipose tissue defined a metabolically-active mature adipocyte subtype characterized by robust expression of genes involved in thermogenesis whose transcriptome was selectively responsive to IL10Rα deletion. Furthermore, single-cell transcriptomic analysis of adipose stromal populations identified lymphocytes as a key source of IL10 production in response to thermogenic stimuli. These findings implicate adaptive immune cell-adipocyte communication in the maintenance of adipose subtype identity and function.

INTRODUCTION

Adipose tissue plays an important role in the maintenance of energy balance in mammals. A chronic imbalance between energy intake and expenditure increases adiposity and leads to obesity and predisposes to the development of metabolic disease (Rosen and Spiegelman, 2014; Wajchenberg, 2000). White adipose tissue (WAT) is essential for triglyceride (TG) storage, whereas thermogenic brown adipose tissue (BAT) dissipates energy as heat through mitochondrial uncoupling mechanisms including uncoupling protein 1 (UCP1) (Cannon and Nedergaard, 2004; Chechi et al., 2013; Saely et al., 2012). A subpopulation of mature adipocytes in certain WAT depots, known as beige adipocytes, also acquires thermogenic capacity in response to cold or hormonal stimuli. Increasing the activity of thermogenic adipocytes in animal models counteracts the development of obesity and diabetes (Cohen et al., 2014; Harms and Seale, 2013; Song et al., 2016; Villanueva et al., 2013). Therefore, a better understanding of the mechanisms controlling adipose thermogenesis could inform the development of new therapies.

In times of metabolic need, white adipocytes mobilize stored lipids through hydrolysis of triglycerides and release of free fatty acid (Zechner et al., 2009). Activation of β-adrenergic receptors (β-ARs) by catecholamines released by the sympathetic nervous system (SNS) is a major physiological inducer of lipolysis and adipose thermogenesis (Bartness et al., 2014; Harms and Seale, 2013; Vitali et al., 2012; Wang et al., 2013). Cold sensation triggers β-AR activation in adipose tissue, resulting in cAMP production and the activation of protein kinase A (PKA) and p38 kinase. These kinases initiate phosphorylation cascades that impinge on C/EBP, ATF, and CREB transcription factors that regulate the expression of gene involved in mitochondrial biogenesis (such as *Ppargc1*) and thermogenesis (such as *Ucp1*) (Harms and Seale, 2013).

Adrenergic stimuli induce lipolysis in adipocytes through PKA-dependent phosphorylation of lipases including hormone-sensitive lipase (HSL) and adipose triglyceride lipase (ATGL) (Duncan et al., 2007; Jaworski et al., 2007; Zechner et al., 2009). Free fatty acid (FA) released from adipocytes can be used by peripheral tissues for mitochondrial respiration. The importance of β-AR-dependent lipid mobilization and thermogenesis is underscored by the observations that genetic deletion of β-ARs or adipocyte-specific loss of ATGL causes a drastic reduction in energy expenditure that predisposes mice to obesity (Bachman et al., 2002; Schreiber et al., 2017).

Clearance of catecholamine is critical in terminating β-adrenergic signals, and local catabolism of catecholamine is an established mechanism for negative regulation of adrenergic signaling in adipose tissue (Camell et al., 2017; Pirzgalska et al., 2017; Song et al., 2019). However, our prior studies revealed an unexpected role for IL10 signaling in the inhibition of β-adrenergic signaling and adipose thermogenesis (Rajbhandari et al., 2018). Mice globally-deficient in IL10 expression have enhanced energy expenditure and are protected from diet-induced obesity. We showed that chromatin accessibility at thermogenic genes in subcutaneous adipose tissue was linked to IL10 signaling; however, whether adipocytes themselves are the primary target for the metabolic effects of IL10 in vivo remains to be established. Here, we show that adipocyte-specific deletion of IL10Rα increases adipose adrenergic signaling, recapitulating the effects of whole-body IL10 deletion. Single nuclei transcriptomics of mature subcutaneous adipocytes identified a thermogenic adipocyte subtype that was enriched in IL10Rα-deficient mice. Additionally, single-cell RNA-sequencing (scRNA-Seq) of adipose stromal populations revealed an increase in IL10-producing adaptive immune cells under

adrenergic stimulation. These results define an immune-adipocyte axis that plays an important role in the modulation of the adipose adrenergic response.

RESULTS

Loss of AdIL10Rα in adipocytes promotes thermogenesis and confers obesity resistance.

We previously reported that global IL10-deficient mice have increased energy expenditure and browning of white adipose tissue (Rajbhandari et al., 2018). To definitively determine whether mature adipocytes are the major cellular targets for these metabolic effects of IL10 we generated adipocyte-specific IL10 receptor α-deficient mice (AdIL10Rα KO) by crossing *Il10ra*$^{FL/FL}$ mice to adiponectin-*Cre* transgenics. We confirmed loss of IL10Rα in adipocytes by western blotting (Fig. 1A). We did not observe a significant difference in body weight between 10 week-old chow-fed AdIL10Rα KO mice and floxed littermate controls (Fig. S1A). However, metabolic cage analysis revealed increased oxygen consumption and energy expenditure in AdIL10Rα KO mice, without changes in locomotion and body mass (Fig. 1 and S1B). To determine if this difference in energy expenditure would protect against diet-induced obesity, we challenged AdIL10Rα KO with high-fat diet (60% calories from fat). After 8-9 weeks of HFD feeding, both male and female AdIL10Rα KO mice were protected against weight gain compared to floxed littermate controls (Fig. 1C, D and S1C). MRI analysis of body composition showed that the difference in body weight was entirely due to a change in fat mass (Fig. 1E). Consistent with these findings, the inguinal WAT (iWAT) of AdIL10Rα KO mice was visibly redder than that of controls, suggesting increased tissue "browning" (Fig. 1F).

To test the influence of the IL10-IL10R axis on adipose adrenergic responses, we exposed AdIL10RαKO and floxed control mice to cold stress (4 °C) for 24 h. Analysis of iWAT gene expression by real-time PCR showed increased expression of *Ucp1*, *Elovl3*, *Ppargc1* and other thermogenic genes, but no change in general adipose markers such as *Fabp4* and *Pparg* in AdIL10Rα KO mice (Fig. 2A). Similar results were observed in AdIL10Rα KO mice treated

with β3-adrenergic agonist (CL 316,243; CL, 1 mg/kg/day for 4 days; Fig. 2B). To gain insight into the global adipose gene expression changes in AdIL10Rα KO mice, we performed RNA-seq on iWAT. We identified 214 genes that were enriched more than 1.5-fold in AdIL10Rα KO mice compared to control mice (presented as a heatmap as a function of percentile expression in Fig. 2C). The data revealed a selective increase in the thermogenic gene program in AdIL10Rα KO mice compared to controls. The gene expression differences between AdIL10Rα KO mice and controls were highly consistent with those observed in global IL10-deficient mice compared to WT controls (Rajbhandari et al., 2018), strongly suggesting that the effects of IL10 on adipose tissue gene expression are mediated predominantly through direct action of IL10 on adipose IL10Rα. Pathway analyses of the differentially expressed genes (DEG) showed positive regulation of lipid metabolism and cold-induced thermogenesis in AdIL10Rα KO mice, further supporting a specific inhibitory effect of IL10Rα signaling on adrenergic-responsive pathways (Fig. S1D). We also noted that several genes that were more highly expressed in control mice compared to AdIL10Rα KOs have been linked to negative regulation of thermogenesis. For example, *Cnotl1* and *Brd2* have been reported to negatively regulate the mRNA stability and transcription of UCP1, respectively (Fig. 2C) (Takahashi et al., 2015). In support of the calorimetric findings, we found increased mitochondrial respiration in the iWAT of AdIL10Rα KO mice compared to controls by Seahorse assays (Fig. 2D).

Identification of thermogenic adipocytes by SNAP-Seq

The data above show that the IL10 acts directly on adipocyte AdIL10Rα to regulate the thermogenic gene program in adipocytes. To further dissect the role of the IL10-IL10R axis in regulating the identity and physiology of mature adipocytes, we performed single-cell analyses.

As there were no prior reports of single primary adipocyte transcriptomics, we optimized a Single Nuclei Adipocyte RNA sequencing approach (SNAP-seq) for assessing gene expression in mature adipocytes derived from mouse iWAT (Fig. 3A and see Experimental Procedures). The critical step in this procedure is the isolation and purification of adipocyte nuclei which overcomes technical obstacles related to the handling of lipid-laden adipocytes. The single nuclei suspension (n ~ 10,000) was subjected to snRNA-Seq using the 10XGenomics platform, and libraries were sequenced with dedicated 400 million reads per sample (Fig. 3A).

We chose to analyze mice exposed to a 24-h cold challenge in these initial studies in order to increase our chance of identifying thermogenic adipocyte populations. We used the 10X genomics data processing and analysis platform to generate cell clusters and identities (see Experimental Procedures). To classify the adipocyte populations based on gene expression, we performed cluster analysis as represented by t-distributed stochastic neighbor embedding (t-SNE) plots. Remarkably, this analysis revealed that the adipocytes from iWAT of chow-fed C57BL/6 mice were highly heterogeneous. We were able to distinguish 14 distinct clusters (Fig. 3B). Importantly, several genes characteristic of mature adipocytes, such as *Fabp4* and *Cd36,* showed an even distribution throughout the clusters (Fig. 3C), confirming that all of the clusters represent populations of mature adipocytes. However, the violin plots in Fig 3C further revealed that each cluster also uniquely express marker genes that were preferentially expressed in individual cluster. The tSNE-plot in Figure 3D further show localized expression of genes in particular cluster. Among all the clusters, we noticed a high enrichment of genes involved in fatty acid metabolism such as *Adrb3* and *Acsl1* in cluster 9. Furthermore, genes encoding β3-AR, HSL, and ATGL were highly overrepresented in this cluster, as were a variety of beige/brown adipocyte markers (Fig. 3E). The gene expression profile of Type 9 adipocytes was indicative of

a highly metabolically active population whose characteristics were potentially consistent with thermogenic "beige" adipocytes.

Identification of a cold-responsive thermogenic "beige" adipocyte population by SNAP-seq

To further test the hypothesis that Type 9 adipocytes were the thermogenic beige population, we subjected mice to different thermogenic conditions, including cold stress (4 °C) for 24 h, 48 h, and 4 days, or treated them with CL for 4 days (1 mg/kg/day). We then performed SNAP-seq on adipocytes derived from iWAT as described above. We performed unbiased aggregated clustering of the processed data for all the conditions as a tSNE-plot (Fig. 4A). The aggregated cluster represents ~54,000 cell and allows us to confidently assign biological function to each cluster. Hence, to infer the biological properties of the cells in each cluster, we performed cell-type pathway enrichment analysis (Gene ontology (GO), KEGG, Reactome, and BIOCARTA) (Table S1) using enriched genes in each cluster based on false discovery rate (FDR) set at <0.05. This analysis revealed that different adipocyte subtypes express distinct genes with important roles in adipose tissue development, insulin signaling, hypoxia signal, inflammation, lipid synthesis and transport, angiogenesis, myogenesis, hormone responses, mitochondrial respiration, and fatty acid metabolic process (shown in Table S1). Type 1 adipocytes appeared to represent classical adipocytes and they expressed genes associated with adipose development, lipid responses, the insulin pathway, and response to corticosteroids (e.g. *Fto, Vldlr, Insr, Apod, Klf9, Sh3pxs2b*); Type 3 adipocytes were enriched for genes involved in blood vessel morphogenesis and angiogenesis; both Type 3 and 14 adipocytes were enriched for genes involved glycolysis. Type 6 and 7 adipocytes were enriched for genes involved in muscle metabolic process and myogenesis; Type 10 adipocytes were

enriched for genes involved in the immune response; Type 11 adipocytes were enriched for cell cycle genes; Type 14 adipocytes were enriched for genes involved in mitochondrial ATP synthesis and respiration. Some adipocyte clusters displayed more commonality in gene expression with others and shared similar biological process, such as the abundant Type 1,2,3 and 7,6 and 17 adipocytes (Fig 5A, and Table S1).

The top 5 enriched pathways determined by FDR from each cell type cluster were selected (from Table S1) and only unique pathways were kept (some top enriched pathways were shared across cell type clusters). Enriched pathways (rows) were clustered with hierarchical clustering. The size of each dot represents the -log10 FDR of the pathway enrichment and the color of each dot corresponds to the fold enrichment of each pathway (red-higher enrichment, grey- lower enrichment). Fig. S2, we report the top 5 scoring pathways for each cell type cluster across all pathway sources (Fig. S2A) or from KEGG pathways (Fig. S2B). Overall, the most striking cluster was the Type 9 adipocytes. Pathways enriched for triglyceride and neutral lipid catabolism, hormone-sensitive lipase (HSL)-mediated triglyceride hydrolysis and PPARα signaling were particularly enriched in type 9 cluster (Fig S2 A,B).

Among all clusters (1-17), we noticed a very distinct sub-clustering of Type 9 adipocytes, with a gradient of adipocyte subtypes in this population from room-temperature (RT) housed mice (top-RED), to mice exposed to cold for 4 days (Middle-Blue), to mice treated with CL (Bottom-Pink) (Figure 4B). Consistent with the data in Fig. 3, aggregated violin plotting showed that genes encoding β3-AR, HSL, ACSL1 were selectively enriched in the Type 9 cluster (Fig 4C and S3 A,B). The tSNE-plot in Figure 4D reveals localized expression of thermogenic genes in cluster 9. Cluster 9 adipocytes from CL- and cold-treated mice showed expression of markers of brown genes such as *Ucp1, Ppargc1a, Cidea, Dio2,* whereas *Adrb3, Lipe, Vegfa, Pnpla2* were

expressed by most of the adipocytes in cluster 9 regardless of thermogenic stimuli (Fig. 4D). Violin plots of thermogenic genes further showed upregulation of genes such as *Ucp1, Ppargc1a,* and *Cidea* in Type 9 adipocytes in mice treated with thermogenic stimuli, confirming these cells as a bona-fide "thermogenic adipocyte" cluster (Fig. 4E). By contrast, genes involved in lipid mobilization such as *Adrb3 and Lipe* were abundant in all Type 9 cells regardless of stimulus, underscoring the relevance of these genes in thermogenic responsiveness and FFA metabolism. *Il10, Il10ra,* and *Il10rb* expression showed a relatively even distribution among mature adipocyte populations (Fig. S3C).

Increased abundance of metabolically active Type 9 adipocytes in AdIL10Rα KO mice.

To probe if IL10 signaling influenced the percentage of thermogenic adipocytes, we exposed both floxed-control and AdIL10Rα KO mice to either cold stress (4°C) for 24 h, 48 h, or 4 days, or treated them with CL (1 mg/kg/day) for 4 days, and performed SNAP-seq on iWAT of these mice. Cluster 9 from the aggregated data showed a progressive increase in the percentage of cells upon exposure to cold for increasing lengths of time (3.4% to 5.7% to 12.1% from 24 h to 48 h to 4 days at 4 °C, respectively) as shown both by tSNE- and dot-plots and treatment of mice with CL even more dramatically increased the abundance of Type 9 cells to 23.5% (Fig. 5A-top and bottom). Dot-plot further show that among all clusters, type 1, 4, and 9 show most changes under different conditions and among them only type 9 adipocyte showed adrenergic-dependent positive increase in cell fractions (Fig. 5A-bottom). We next compared data from control and AdIL10Rα KO mice, and in agreement with the whole tissue RNA-seq data presented above, adipocytes from AdIL10Rα KO mice showed a specific increase in the population of thermogenic adipocytes (cluster 9) under both basal conditions (RT) and in

response to thermogenic stimuli (cold exposure or CL treatment) (Fig. 5B). The dot-plot in Figure 5C shows that the overall pattern of adipocyte cluster enrichment did not differ from Figure 5A-bottom and only type 9 adipocytes showed a positive shift in cell fraction upon IL10R depletion, except for 48 h cold exposure where we observed unexpected 4% decrease in cell fraction.

Type 9 adipocytes from AdIL10RαKO mice were more metabolically active and showed increased expression of genes linked to mitochondrial activity, energy derivation from FFA, and positive regulation of cold-induced thermogenesis (Fig. S4A). A Volcano plot of the data revealed that genes involved in lipid mobilization and adipose thermogenesis (such as *Lipe, Nr1d1, Oplah, Nfkbia, Pck1, Cebpb, Vegfa, Angptl4*) were increased, and genes correlated with obesity and adiposity such as (*Nrip1, Lpl, Zbtb20, Acss2*) were decreased in iWAT adipocytes from AdIL10RαKO mice compared to controls (Fig. 5D). However, not all adipogenic and thermogenic genes were different between AdIL10Rα KO and control adipocytes. For example, pan-adipocyte genes such as *Cd36, Fabp4*, and *Aqp1* were similarly expressed between cells of both genotypes (Fig. S4B). Overall, our SNAP-seq data reveal previously unappreciated heterogeneity of mature adipocytes in subcutaneous adipose tissue and point to the existence of distinct cell populations with potentially specialized biological functions. These data further show that IL10 signaling in fat tissue targets a distinct, highly metabolically active and thermogenic adipocyte population.

scRNA-Seq of iWAT stromal vascular fraction reveals a role for IL10-expressing adaptive immune cells in regulation of adipose thermogenesis

Prior bone marrow transplantation experiments had shown that IL10 produced by one or more hematopoietic cell types could rescue the thermogenic phenotype of global IL10-deficient mice (Rajbhandari et al., 2018). Therefore, we examined changes in non-adipocyte cells types within iWAT in the setting of thermogenic stimuli to evaluate their potential contribution to IL10/IL10R signaling. We treated WT mice with saline or β3-adrenergic agonist (CL; 1 mg/kg/day) for 4 days, separated iWAT stromal cells from adipocytes, and performed scRNA-Seq on ~10,000 isolated stromal vascular cells (SVF) per mouse as described in Experimental Procedures. t-SNE plotting of the data revealed 12 major cell clusters (Fig. 6A). Further subclustering analysis based on known cell marker genes identified four clusters of adipocyte precursor cells (APCs), four clusters of B cells, three clusters of macrophages, and four clusters of T cells (Fig. 6A).

To gain insight into the remodeling of stromal cells under adrenergic stress, we segregated the cumulative tSNE-plot into CL and saline treatment. The tSNE and dot plots in Fig. 6B and 6C reveal a relative depletion of APCs and a major increase in B-cell populations in iWAT upon CL treatment. Since adaptive immune cells (T- and B-cells) are major potential producers of IL10 (Saraiva and O'Garra, 2010), we further examined IL10 transcript levels in our data set. tSNE-plotting showed that total IL10 transcripts increased ~3-fold upon CL treatment in B-cell clusters (Fig. 6D). To quantitatively determine IL10 transcript levels in saline and CL-treated conditions, we plotted fold change of the ratio of CL and saline as a function of p value. Compared to saline (represented by dotted line) *Il10* was markedly upregulated in T- and B-cell populations (Fig. 6E).

To test the possibility that production of IL10 by iWAT-resident T and B cells might contribute to the regulation of thermogenesis, we treated WT or functional T- and B-cell–

deficient SCID mice (Bosma et al., 1988) with CL or exposed them to 4 ºC for 24 h. In agreement with our hypothesis, the thermogenic gene program was enhanced in the iWAT of SCID mice compared to controls (Fig. 7A, B). Accordingly, SCID mice also had higher EE and oxygen consumption and decreased RER, as measured by metabolic chamber studies. (Fig. 7C). Collectively, these results suggest that lymphocytes are an important source of the IL10 acting on adipocyte IL10 receptors during thermogenesis.

DISCUSSION

The influence of inflammation on obesity and adipose insulin resistance has been studied extensively; however, the role of adipose-resident immune cells in regulating the balance between adiposity, lipid mobilization, and thermogenesis is incompletely understood. We previously reported that hematopoietic-secreted IL10 inhibits adrenergic signaling-mediated lipid mobilization and thermogenesis (Rajbhandari et al., 2018). Here we provide evidence from scRNA-seq analysis of both adipose stromal-vascular cells and mature adipocytes indicating that adrenergic stimulation causes an increase in the abundance of IL10-secreting adaptive immune cells, and that this cytokine acts directly on the IL10Rα complex in mature adipocytes to antagonize thermogenesis. Genetic ablation of IL10Rα in adipocytes increases the browning of white adipose tissue and selectively enhances thermogenic gene expression, defining mature adipocytes as the primary target of the metabolic actions of IL10. Our SNAP-seq data further revealed that adipose tissue is composed of surprisingly complex subpopulation of adipocytes, including distinct subtypes whose gene expression suggests they are subspecialized for different processes, including lipogenesis and thermogenesis. Deletion of IL10Rα selectively increases the subpopulation of metabolically active, thermogenic adipocytes.

The immune system plays an important role in maintaining adipose homeostasis. Prior studies have shown that signaling from both innate and adaptive immune cells influences lipid handling, adipocyte size and function, and whole body lipid homeostasis (Bapat et al., 2015; Schaffler and Scholmerich, 2010; Sell et al., 2012; Wernstedt Asterholm et al., 2014). In a proinflammatory state, as seen in adrenergic stress, cancer cachexia, and burn victims, adipose tissue undergoes remodeling that activates lipid mobilization and thermogenesis which can lead to lipodystrophy (Patsouris et al., 2015; Petruzzelli et al., 2014). One established mechanism to

block uncontrolled lipolysis is through catabolism of catecholamines. Sympathetic-associated macrophages, NRLP3 inflammasomes, and OCT3 have all been shown to enhance catecholamine clearance in adipose tissue (Camell et al., 2017; Pirzgalska et al., 2017; Song et al., 2019). Immune cells also could counteract adrenergic signaling by releasing factors that prevent excessive lipolysis and thermogenesis and thereby direct adipocytes to reserve energy in the setting of starvation or infection. This idea is supported by our scRNA-seq studies on iWAT SVFs of mice under adrenergic stress. Mice treated with β3-adrenergic agonist have expanded adaptive immune cell populations and a 3-fold increase the abundance of IL10 transcript in adipose SVF. Increased production of IL10 in the microenvironment could antagonize adrenergic-mediated thermogenesis, potentially providing a mechanism whereby immune cells help to maintain lipid homeostasis in the setting of energy demand.

A recent study has shown that deletion of Oct coactivator from B-cells (OcaB), which is essential for B-lymphocyte maturation and development, promotes adipose browning and protects mice from age-induced insulin resistance (Carter et al., 2018). Similarly, deletion of anti-inflammatory Tregs also protect mice from age-induced obesity and insulin resistance (Bapat et al., 2015). We showed here that the absence of IL10-secreting adaptive immune cells in mice also leads to enhanced adipose thermogenesis, a finding consistent with the phenotypes of both IL10 KO and AdIL10Rα KO mice.

To more deeply interrogate the effect of IL10 signaling on adipocyte identity and function, we performed SNAP-seq of adipocytes from iWAT. Although prior studies have used FACS and immortalized clonal preadipocytes to assess different types of adipocytes in various adipose tissue depots (Hagberg et al., 2018; Lee et al., 2019), to our knowledge, this is the first report of rigorous single nuclei RNA-Seq of adipocytes in the setting of a thermogenic challenge.

Our data revealed distinct clusters reflecting subsets of mature adipocytes with differential gene expression. Our data show that the mature tissue adipocyte population is much more heterogeneous than previously appreciated. We categorized by 14 distinct subsets of mature adipocytes that appear to be specialized to participate in at least partially distinct metabolic pathways. These findings suggest that different functions of adipose tissue may be executed by different cell populations, rather than similar cell populations performing diverse functions. Further studies will be needed to test this idea.

Interestingly, Type 9 adipocytes were highly metabolically active and thermogenic, and we speculate that this cluster corresponds to the so-called "beige" adipocyte population. Violin plots of the Type 9 cluster showed selective expression of genes involved in lipid mobilization, such as *Adrb3, Acsl2, Lipe, Pnpla2*, and brown/beige-associated genes such as *Ucp1, Cidea, Dio2,* and *Clstn3*. The identity of this cluster was further confirmed by performing snRNA-seq on adipocytes from mice at RT, exposed to cold for various times, or treated with CL. We saw a gradual increase in the percentage of Type 9 adipocytes with increasing thermogenic stimulus.

Interestingly, we also noticed distinct sub-clustering of Type 9 adipocytes within the cluster. Cells expressing genes involved in lipolysis had an even distribution, whereas cells with higher expression of brown/beige genes were subclustered together after 4 days of cold or CL treatment. This data suggests that *Adrb3*-expressing adipocytes have varying browning capacity. We also noticed that the subclustering patterns of cold-exposed versus CL-treated Type 9 adipocytes were also different. This likely reflects different transcriptional responses to cold exposure and pharmacological adrenergic receptor activation. DEG analysis of AdIL10Rα KO and control adipocytes showed that ablation of IL10Rα leads to differential enrichment of adipocyte populations. Type 9 adipocytes appear to be enriched in genes that are highly

expressed in AdIL10Rα KO compared to control iWAT. Furthermore, AdIL10Rα KO adipocytes are more metabolically active and have heightened response to adrenergic stimulation compared to controls. These data suggest that deletion of IL10Rα from adipocytes leads to the selective enrichment of metabolically active adipocytes that could ultimately lead to increased response to adrenergic signaling and enhanced thermogenesis.

In conclusion, these data provide insight into crosstalk between IL-10-secreting immune cells and adipocytes within adipose tissue, as well as into the complexity of the transcriptional response to adrenergic signaling in mature adipocytes. A better understanding of the pathways influencing the development and phenotypic transformation of Type 9 adipocytes could ultimately lead to strategies to increase energy expenditure and protect against diet-induced obesity.

AUTHOR CONTRIBUTIONS

P.R., D.A, A-C.F., I.S.A., G.D., B.J.T, L.V., S.D.L., performed the experiments. P.R., X.Y., and P.T. designed the experiments and interpreted the data. P.R. and P.T. wrote the manuscript. P.T. X.Y., K.R., and S.T.S. supervised the study.

ACKNOWLEDGEMENTS

We thank UCLA Broad Stem Cell Research Center Core for sequencing and Technology Center for Genomics & Bioinformatics for single cell sequencing. This work was supported by NIH grants K99DK114571 (P.R.), HL090533 (K.R. and P.T.), DK104363 and UL1TR001881 (X.Y.), R01GM086372 (S.T.S.), and DK063491 (P.T.). A-C. F. is funded by the Tri-Service General

Hospital, National Defense Medical Center, Taipei, Taiwan. The funders had no role in study design, data collection and interpretation, or the decision to submit the work for publication.

CONFLICTS OF INTEREST

The authors declare no conflicts of interest

EXPERIMENTAL PROCEDURES

Animal Studies

Breeding pairs of *Il10RaF/F*mice (#028146), Adiponectin CRE (#010803), C57BL/6 SCID (#001913) and C57BL/6 WT controls (#000664) were acquired from Jackson Laboratory and maintained in a pathogen-free barrier-protected environment (12:12 h light/dark cycle, 22°C-24°C) at the UCLA animal facility. Experimental mice were sacrificed at ages mentioned in figure legends for gene expression analysis. For the time course cold exposure experiment, WT mice at 8-10 weeks of age were singly housed at 4°C room in a non-bedded cage without food and water for first 6 h; thereafter food, water, and one cotton square were added. For the 24 h harvest, 3 h before harvest, food, water, and cotton square were removed and then mice were harvested. For the 48 h and 4-day cold exposure, cages were changed daily with new cotton squares and 3 h before the time of harvest, the food, water, and cotton square were removed. For β-adrenergic stimulation experiments, mice were intraperitoneally injected with β3-adrenergic agonist (CL 316,243; CL, at 1 mg/kg/day for 4 days) or saline. For the diet study, 10-week-old *Il10ra*$^{F/F}$ and AdIL10RαKO mice were fed a 60% high-fat diet (Research Diets) for the indicated times. Mouse weights were measured every week and food was replaced weekly. At the end of the experiment, iWATs were resected for gene expression analysis. Indirect calorimetry was

performed using a Columbus Instruments Comprehensive Lab Animal Monitoring System (CLAMS, Columbus Instruments). Animals were placed individually in chambers for 3 consecutive days at ambient temperature (26.5°C) with 12 hr light/dark cycles. Animals had free access to food and water. Respiratory measurements were made in 20 min intervals after initial 7-9 hr acclimation period. Energy expenditure was calculated from VO2 and RER using the Lusk equation, EE in Kcal/hr = (3.815 + 1.232 X RER) X VO2 in ml/min. CLAMS data were analyzed by CALR web-based software (Mina et al., 2018). Animal experiments were conducted in accordance with the UCLA Institutional Animal Care and Research Advisory Committee.

RNA-Seq

Total RNA was prepared as described (Tong et al., 2016). Strand-specific libraries were generated from 500 ng total RNA using the TruSeq Stranded Total RNA Library Prep Kit (Illumina). cDNA libraries were single-end sequenced (50bp) on an Illumina HiSeq 2000 or 4000. Reads were aligned to the mouse genome (NCBI37/mm9) with TopHat v1.3.3 and allowed one alignment with up to two mismatches per read. mRNA RPKM values were calculated using Seqmonk's mRNA quantitation pipeline. A gene was included in the analysis if it met all the following criteria: the maximum RPKM reached 4 at any time point, the gene length was >200bp, and for in-vitro studies was induced at least 3-fold from Day 0 samples, and the expression was significantly different from the basal (P<0.01) as determined by the DESeq2 package in R Bioconductor. P-values were adjusted using the Benjamini-Hochberg procedure of multiple hypothesis testing (Benjamini and Hochberg, 1995)

scRNA-Seq of adipose stromal vascular fraction (SVF) population

Single cell isolation from SVF- Inguinal white adipose tissue (iWAT) from mice treated with saline or CL were dissected and placed on sterile 6-well tissue culture plate with ice-cold 1X DPBS. Fat pads were blotted on a napkin to removed excess liquid. Tissues were cut and minced with scissors and placed in 15 ml conical tubes containing digestion buffer (2 ml DPBS and Collagenase II at 3 mg/ml; Worthington Biochemical, Lakewood, NJ, USA) and incubated at 37 °C for 40 min with gentle shaking at 100rpm. Following tissue digestion 8 ml of resuspension media (DMEM/F12 with glutamax supplemented with 15%FBS and 1% pen/strep; Thermo Scientific, CA) was added to stop enzyme activity. The digestion mixture was passed through 100 µm cell strainer and centrifuged at 150 x g for 8 min at room temperature. The pellet was resuspended and incubated in RBC lysis buffer (Thermo Scientific, CA) for 3 min at room temperature to remove red blood cells followed by centrifugation at 150 x g for 8 min. The pellet was resuspened in resuspension media and spun down again at 150 x g for 8 min. Finally, the cell pellet was resuspended in 1 ml of 0.01% BSA (in DPBS). This final cell suspension solution was passed through a 40 µm cell strainer (Fisher Scientific, Hampton, NH, USA) to discard debris and cell number was counted for Drop-Seq application.

Drop-seq single cell barcoding and library preparation- The Drop-seq protocol from Macosko et al and version 3.1 of the online Drop-seq protocol [http://mccarrolllab.com/download/905/] was followed with minor modifications to generate STAMPs (single-cell transcriptomes attached to microparticles) and cDNA libraries (Arneson et al., 2018; Macosko et al., 2015). Briefly, to create oil droplets with barcoded cells, single cell suspensions (100 cells/µl), EvaGreen droplet generation oil (BIO-RAD, Hercules, CA, USA), and ChemGenes barcoded microparticles (ChemGenes, Wilmington, MA, USA) were co-flowed

through a FlowJEM aquapel-treated microfluidic device (FlowJEM, Toronto, Canada) at the recommended flow speeds (oil: 15,000 µl/hr, cells: 4000 µl/hr, and beads 4000 µl/hr). After STAMP generation, oil droplets were broken, and cDNA synthesis was performed. To obtain enough cDNA for library preparations the Drop-seq protocol was followed with the following modifications. For the PCR step, 4000 beads were used per tube, the number of cycles was changed to 4 + 11 and multiple PCR tubes were pooled. cDNA library concentration and quality were assessed using the Agilent TapeStation system (Agilent, Santa Clara, CA, USA). The samples were then tagmented using the Nextera DNA Library Preparation kit (Illumina, San Diego, CA, USA) and multiplex indices were added. After another round of PCR, the samples were assessed on a Tapestation high sensitivity DNA screentape (Agilent, Santa Clara, CA, USA) for library quality before sequencing.

Illumina high-throughput sequencing of Drop-seq libraries- Molar concentrations of the Drop-seq libraries were quantified using the Qubit Fluorometric Quantitation system (ThermoFisher, Canoga Park, CA, USA) and library fragment lengths were estimated using a Tapestation high sensitivity DNA screentape (Agilent, Santa Clara, CA, USA). Samples were normalized by concentration and then pooled appropriately. Pooled libraries were then sequenced on an Illumina HiSeq 4000 (Illumina, San Diego, CA, USA) instrument using the Drop-seq custom read 1B primer (GCCTGTCCGCGGAAGCAGTGGTATCAACGCAGAGTAC) (IDT, Coralville, IA, USA) and PE100 reads were generated. Read 1 consists of the 12 bp cell barcode, followed by the 8 bp UMI, and the last 80 bp on the read are not used. Read 2 contains the single cell transcripts.

Drop-seq data pre-processing and quality control- Demultiplexed fastq files generated from Drop-seq were processed to digital expression gene matrices (DGEs) using Drop-seq tools version 1.13 (https://github.com/broadinstitute/Drop-seq) and dropEst (Petukhov et al., 2018). The workflow is available as modified version of the snakemake-based dropSeqPipe (https://github.com/Hoohm/dropSeqPipe) workflow and is available on github (https://github.com/darneson/dropSeqPipeDropEST). Briefly, fastq files were converted to BAM format and cell and molecular barcodes were tagged. Reads corresponding to low quality barcodes were removed and any occurrence of the SMART adapter sequence or polyA tails found in the reads was trimmed. These cleaned reads were converted back to fastq format to be aligned to the mouse reference genome mm10 using STAR-2.5.0c. After the reads were aligned, the reads which overlapped with exons, introns, and intergenic regions were tagged using a RefFlat annotation file of mm10. To make use of reads aligning to intronic regions, which are not considered in Drop-seq tools v1.13, we used dropEst to construct digital gene expression matrices from the tagged, aligned reads where each row in the matrix is the read count of a gene and each column is a unique single cell. The count values for each cell were normalized by the total number of UMIs in that cell and then multiplied by 10,000 and log transformed. Single cells were identified from background ambient mRNA using thresholds of at least 700 transcripts and a maximum mitochondrial fraction of 10%.

Identification of cell clusters- The Seurat R package version 3.0.0.9000 (https://github.com/satijalab/seurat) was used to project all sequenced cells onto two dimensions using t-SNE and Louvain (Blondel et al., 2008; Laurens van der Maaten, 2008) clustering was used to assign clusters. The optimal number of PCs used for t-SNE/UMAP

dimensionality reduction and Louvain clustering was determined using the Jackstraw permutation approach and a grid-search of the parameters. Similarly, the density used to assign clusters was identified using a parameter grid search.

Identification of marker genes of individual cell clusters- We defined cell cluster specific marker genes from our Drop-seq dataset using the FindConservedMarkers function in Seurat across all the samples. Briefly, a Wilcoxon Rank Sum Test is run within each sample and a meta p-value across all samples is computed to assess the significance of each gene as a marker for a cluster. Within each sample, the cells are split into two groups: single cells from the cell type of interest and all other single cells. To be considered in the analysis, the gene had to be expressed in at least 10% of the single cells form one of the groups and there had to be at least a 0.25 log fold change in gene expression between the groups. This process was conducted within each sample separately, and then a meta p-value was assessed from the p-values across all samples. Multiple testing was corrected using the Benjamini-Hochberg method on the meta p-values and genes with an FDR < 0.05 were defined as cell type specific marker genes.

Resolving cell identities of the cell clusters- We used two methods to resolve the identities of the cell clusters. First, we used known cell-type specific markers curated from literature, single cell atlases, previous studies in the SVF and PBMCs, and from Immgen (immgen.org) to find distinct expression patterns in the cell clusters (Burl et al., 2018; Chen et al., 2018; Han et al., 2018; Hepler et al., 2018; Schaum et al., 2018; Stoeckius et al., 2017; Zhang et al., 2018). A cluster showing unique expression of a known marker gene can be used to identify that cell type. To consider more than a single gene, we evaluated the overlap between known cell type marker genes with the marker genes identified in our cell clusters using

FindConservedMarkers. Significant overlap was assessed using a Fisher's exact test with Bonferroni correction for multiple testing. The two methods showed consistency in cell identity determination.

Single Nuclei Adipocyte RNA-Sequencing (SNAP-Seq)

Adipocyte nuclei isolation from iWAT- 200-400 mg of inguinal white adipose tissues (iWAT) from mice exposed to conditions mentioned in the text were placed on sterile 6-well tissue culture plate with ice-cold 1XPBS. Fat pads were blotted on a napkin to removed excess liquid. Tissues were cut and minced with scissors and were placed in 15ml conical tubes containing digestion buffer (DPBS and Collagenase D at 9.8 mg/ml; Sigma, MO) at incubated at 37 °C for 45 mins with gentle shaking at 100 rpm. 10 ml of resuspension media (DMEM/F12 with glutamax supplemented with 15% FBS and 1% pen/strep; Thermo Scientific, CA) was added to digested solution and slowly inverted 5 times. The digestion mixture was centrifuged at 200 x g for 5mins at RT. Floating adipocytes were collected using P1000 pipet with half cut P1000 tip. Adipocytes were transferred to a new 15 ml tube and kept on ice for 5 mins. Excess liquid was aspirated using 1 ml syringe and adipocytes were then washed with 1ml DPBS and the suspension was spun down at 200 g for mins at RT. Spun down liquid was aspirated using 1 ml syringe and adipocyte nuclei were isolated using Minute nuclei and cytosol isolation kit for adipose tissue using manufacture's instruction (Invent Biotechnologies, MN) with modifications. Briefly, adipocytes were slowly resuspended in 600 µl nuclei lysis buffer (N/C Buffer) and lysate was transferred to a filter cartridge with collection tube and incubated at -20°C freezer for 20 min with cap open. After incubation, the tube was centrifuged at 2000 rpm for 2 min at 4 °C. The filter cartridge was discarded without agitation and the collection tube was immediately centrifuged at 4000 rpm for 4 min at 4 °C. Supernatant was gently removed using P200 pipet

without touching the side walls. Nuclei were resuspended in 30 ul of nuclei resuspension buffer (DPBS+0.1%BSA) per 200-400 mg of iWAT (i.e. one 8-10 week chow fed mouse). For SNAP-seq, 2-3 mice were combined and 60 µl of nuclei suspension was transferred to a new 2 ml tube and resuspended with 500-700 µl of nuclei resuspension buffer and filtered using 40 µm cell strainer (Flowmi Cell Strainer, Belart, NJ) twice to get clean single nuclei suspension. As shown in Figure 3A, for quality control, nuclei were first DAPI stained and then filtered or FACS sorted to get single nuclei suspension. After microfluidic partitioning in 10xGenomics platform (see below), nuclei lysis was checked by observing oil emulsion under fluorescent microscope for DAPI diffusion.

Adipocyte Single Nuclei barcoding and library preparation- Approximately 10,000 nuclei were loaded onto Single Cell 3' Chip (10xGenomics, CA) per channel with an expected recovery to 4000-7000 nuclei. The Chip was placed on a 10XGenomics Instrument to generate single nuclei gel beads in emulsion (GEMs). For optimal nuclei lysis, GEMs were incubated on ice for 50 mins. After incubation, single nuclei RNA-Seq libraries were prepared using Chromium Single Cell 3' Library and Cell Bead Kit) according to manufacturer's instruction.

Illumina high-throughput sequencing libraries-The 10X genomics library molar concentration was quantified by Qubit Fluorometric Quantitation (ThermoFisher, Canoga Park, CA, USA) and library fragment length was estimated using a TapeStation (Aligent, Santa Clara, CA, USA). Sequencing was performed on an Illumina HiSeq 4000 (Illumina, San Diego, CA, USA) instrument with PE100 reads and an 8 bp index read to multiplexing. With the version 3 chemistry, the first 26bp of Read 1 consist of the cell barcode and the UMI, and the last 74 bp on the read are not used. Read 2 contains the single cell transcripts.

SNAP-Seq data pre-processing and quality control-Digital gene expression matrices (DGEs) in sparse matrix representation we obtained using 10x Genomics' Cell Ranger v3.0.2 software suite. Briefly, .bcl files obtained from the UCLA Broad Stem Cell Research Center sequencing core were demultiplexed and converted to fastq files using the mkfastq function in Cell Ranger which wraps Illumina's bcl2fastq v2.19.1.403. The counts function in Cell Ranger was used to generate DGEs from the fastq files. Briefly, the resulting fastq files are aligned to a 10x supplied mm10 reference genome (mm10-3.0.0) using STAR and reads are identified as either exonic, intronic, or intergenic using the supplied 10x Genomics GTF file. To determine cell barcodes, the counts function in Cell Ranger implements an algorithm based on EmptyDrops (Lun et al., 2019). Only reads which align to exonic regions were used in the resulting DGE. The count values for each cell were normalized by the total number of UMIs in that cell and then multiplied by 10,000 and log transformed. Single cells were identified from background ambient mRNA using thresholds of at least 200 genes and a maximum mitochondrial fraction of 10%.

Identification of adipocyte clusters-The Seurat R package version 3.0.0.9000 (https://github.com/satijalab/seurat) was used to project all sequenced cells onto two dimensions using t-SNE/UMAP and Louvain clustering was used to assign clusters. The optimal number of PCs used for t-SNE dimensionality reduction and Louvain clustering were determined using the Jackstraw permutation approach and a grid-search of the parameters. Similarly, the density used to assign clusters was identified using a parameter grid search.

Identification of marker genes of individual adipocyte clusters- We defined cell cluster specific marker genes from our 10x Genomics dataset using the FindConservedMarkers function in Seurat across all the samples. Briefly, a Wilcoxon Rank Sum Test is run within each sample and a meta p-value across all samples is computed to assess the significance of

each gene as a marker for a particular cluster. Within each sample, the cells are split into two groups: single cells from the cell type of interest and all other single cells. To be considered in the analysis, the gene had to be expressed in at least 10% of the single cells form one of the groups and there had to be at least a 0.25 log fold change in gene expression between the groups. This process was conducted within each sample separately, and then a meta p-value was assessed from the p-values across all samples. Multiple testing was corrected using the Benjamini-Hochberg method on the meta p-values and genes with an FDR < 0.05 were defined as cell type specific marker genes.

Resolving cell identities of the cell clusters- Two methods were used to aid in resolving the identities of the cell type clusters. First, KEGG, Reactome, BIOCARTA, GO Biological Processes, and Hallmark gene sets were obtained from MSigDB. To identify pathways which had significant enrichment of our cell type marker genes, we used a hypergeometric test, followed by multiple testing correction with the Benjamini–Hochberg method. We also adapted the method proposed by Zywitza *et al.* to get a single cell level score for each pathway (Zywitza et al., 2018). Briefly, the expression of each gene was linearly transformed to (0,1) and the average gene expression of all genes for each gene set was computed to represent the score for that gene set. We then identified the top scoring gene sets which were representative of each cell type.

Real time qPCR

Total RNA was isolated using TRIzol reagent (Invitrogen) and reverse transcribed with the iScript cDNA synthesis kit (Biorad). cDNA was quantified by real-time PCR using SYBR Green Master Mix (Diagenode) on a QuantStudio 6 instrument (Themo Scientific, CA). Gene expression levels were determined by using a standard curve. Each gene was normalized to the

housekeeping gene 36B4 and was analyzed in duplicate. Primers used for real-time PCR are available upon request.

Western blotting

Whole cell lysate or tissue lysate was extracted using RIPA lysis buffer (Boston Bioproducts) supplemented with complete protease inhibitor cocktail (Roche). Proteins were diluted in Nupage loading dye (Invitrogen), heated at 95°C for 5 min, and run on 4–12% NuPAGE Bis-Tris Gel (Invitrogen). Proteins were transferred to hybond ECL membrane (GE Healthcare) and blotted with IL10Rα (AF-474-SP, R&D Systems), αTubulin (CP06, Calbiochem), Actin (A2066, Sigma-Aldrich),

Cellular and mitochondrial respiration

Mitochondria were isolated from fresh tissues and immediately used in a XF24 analyzer as previously described (Rogers et al., 2011). Briefly, mitochondria were isolated in MSHE+BSA buffer using a 800g/8000g dual centrifugation method and resuspended in MAS buffer. Protein concentration was determined using a Bradford Assay reagent (Bio-Rad) and 20 µg of protein were seeded per well by centrifugation. Coupling and electron flow assays were performed as described (Rogers et al., 2011). For the coupling assay, basal oxygen consumption rate (OCR) was measured in the presence of 10 mM succinate and 2 µM rotenone, and after sequential addition of 4 mM ADP (Complex V substrate), 2.5 µg/ml oligomycin (Complex V inhibitor), 4 µM FCCP (mitochondrial uncoupler) and 4 µM antimycin A (Complex III inhibitor). For electron flow assays, basal OCR was measured in presence of 10 mM pyruvate (Complex I substrate), 2 mM malate and 4 µM FCCP, and after sequential addition of 2 µM rotenone

(Complex I inhibitor), 10 mM succinate (Complex II substrate), 4 μM antimycin A (Complex III inhibitor) and 1mM TMPD containing 10 mM ascorbate (Complex IV substrate).

Statistics

All data are presented as mean ± SEM and analyzed using Microsoft Excel and Prism (Graphpad). Student's t test with Welch's correction was used for single variable comparison between two groups. One-way ANOVA followed by Dunnett post hoc test was used for multiple comparisons versus the control group. Two-way ANOVA followed by Bonferroni posttests was used to examine interactions between multiple variables. Statistical significance for CLAMS study was determined by multiple regression analysis (ANCOVA). $p < 0.05$ was considered to be statistically significant and is presented as * $p < 0.05$, ** $p < 0.01$, *** $p < 0.001$, or **** $p < 0.0001$.

FIGURE LEGENDS

Figure 1. Ablation of IL10Rα in adipocytes increases energy expenditure and protects mice from diet-induced obesity.

(A) Immunoblot analysis of IL10Rα expression in SVF and adipocyte fractions of iWAT from chow-fed 10 week-old mice. (B) Oxygen consumption (VO_2, ml/hr), energy expenditure (EE, kCal/hr), and respiratory exchange ratio (RER) of chow-fed 10-week-old IL10RαF/F and AdIL10Rα KO mice were analyzed in Columbus Oxymax metabolic chambers (12 h light/dark cycles, 72 hr total duration, each light/dark bar represents 12 h duration). N = 9,7. Statistical analysis was performed using ANCOVA. (C) External appearance of representative 9 week HFD-fed mice. (D) Body weight of mice fed chow diet for 10 weeks and then 60% high-fat diet (HFD) for 9 weeks. N = 13, 7. (E) Fat and lean mass of mice in D fed HFD for 6 weeks. (F) Internal and gross appearance of iWAT from representative IL10RαF/F and AdIL10RαKO mice. *, $p<0.05$

Figure 2. IL10R deficiency promotes adipose tissue browning.

(A and B) Real-time PCR analysis of gene expression in iWAT from 10 week 24 h cold-exposed (A) or CL 1 mg/kg/day for 4 days; B) IL10RαF/F and AdIL10RαKO mice. N=5,5. *, $p<0.05$; **, $p<0.01$; ***, $p<0.0001$. (C) Heatmap representation of genes that changed >1.5-fold (p-value <0.01) as a function of percentile expression by RNA-Seq of iWAT from 10 week-old 24 h cold-exposed IL10Rα and AdIL10Rα KO mice. Genes are grouped as upregulated (Red) or downregulated (Blue). (D) Average oxygen consumption rate (OCR) in coupling (left) and electron flow (right) assays of mitochondria isolated from iWAT of mice in (A).

Figure 3. SNAP-seq reveals heterogeneity of tissue adipocytes from iWAT.

(A) Workflow showing DAPI-stained nuclei pre- and post-FACS/filtration that underwent microfluidic partitioning and library preparation in the 10X genomics platform followed by sequencing using an Illumina HiSeq 4000. (B) tSNE-plot showing 14 clusters from ~6000 adipocytes derived from iWAT of mice exposed to cold for 24 h. Each colored dot is an adipocyte assigned to a cluster based on transcriptomic signature. (C) Normalized expression values of the top two adipocyte subtype-specific cluster genes from (B) plotted as violin plots with clusters as rows and genes as columns. (D) tSNE-plot showing cluster-specific expression of selected marker genes from (C). (E) Normalized expression values of indicated genes in subtype-specific clusters plotted as violin plots with clusters as rows and genes as columns. Black arrow is pointing toward metabolically active Type 9 adipocyte cluster and enriched gene.

Figure 4. Transcriptomic visualization of thermogenic adipocytes in iWAT

(A) Aggregated tSNE-plot showing 17 clusters from ~54,000 adipocytes derived from iWAT of mice at RT, cold-exposed (24 h, 48h, and 4 days), or treated with CL for 4 days at 1mg/kg/day. Each colored dot is an adipocyte that falls into a c luster based on transcriptomic signature. (B) tSNE-plot showing indicated treatment-dependent sub-clustering of aggregated clusters shown in (A). Black arrow indicates the Type 9 adipocyte cluster. (C) Normalized expression values of the top two adipocyte subtype-specific cluster genes from (A and B) plotted as violin plots with clusters as rows and genes as columns. (D) tSNE-plot showing distribution of indicated genes from adipocytes from (A). (E) Normalized expression values of indicated genes in the Type 9 adipocyte cluster under different treatment condition plotted as violin plots with treatment conditions as rows and genes as columns.

Figure 5. Enrichment of the thermogenic adipocyte cluster in IL10Rα-depleted mice.

(A) Top: tSNE-plot showing percentage of clusters from aggregated (All) or from indicated treatments. Bottom: Colored dot plot showing percentage of fractions plotted in y-axis and cell types in x-axis under indicated conditions. (B) tSNE-plot showing differences in percentage of clusters between adipocytes from iWAT from control and AdIL10Rα KO mice under RT, 24 h, 48h or 4 days cold exposure, or CL treated conditions. (C) Colored dot plot showing percentage of fractions plotted in y-axis and cell types in x-axis under indicated conditions and genotype. N deonotes Adipoq-Cre-Negative IL10RαF/F (IL10RαF/F) and P denotes Adipoq-Cre-Positive (AdIL10Rα KO) mice. (D) Volcano plot showing adipocyte gene expression differences between indicated mice from cluster 9. The Log2Fold Change (FC) ratio of floxed control vs. AdIL10Rα KO was plotted as a function of log10 p-value, with select genes indicated with text. Black arrow indicates the Type 9 adipocyte cluster.

Figure 6. scRNA-Seq reveals an increase in adaptive immune cells under adrenergic stress.

(A) Aggregated tSNE-plot of combined ~10,000 SVF cells isolated from iWAT of mice treated with CL or saline for 4 days. Colored dots are cells assigned to clusters based on similar transcriptomic signatures and these clusters correspond to specific cell-types. (B) Segregated tSNE-plot from (A) showing percentage of cell-types between control (Saline) and β3-agonist CL-treated mice. The tSNE-plot also shows differences in percentage of clusters between control and CL-treated mice. Black arrows indicate major B-cell population. (C) Colored dot plot showing percentage of fractions plotted in y-axis and cell types in x-axis under indicated conditions. (D) tSNE-plot showing cells expressing *Il10* in control and CL-treated mice. Black arrows indicate major cell clusters with *Il10* expression. (E) Dot plot showing expression levels

of *Il10* in indicated cells comparing control and CL-treated mice. The Log2Fold Change (FC) ratio of saline vs. CL was plotted as a function of log10 p-value and indicated as different sizes of dots. Fold-change and p-value was compared with saline condition represents as a dotted line.

Figure 7. Increased adipose thermogenesis and EE in lymphocyte-deficient mice

(A and B) Real-time PCR analysis of gene expression in iWAT from chow-fed 10 week 24 h cold-exposed (A) or CL (1 mg/kg/day for 4 days (B) mice. (C) Bar graphs and scatter plot (Light cycle) showing oxygen consumption, energy expenditure, carbon dioxide production, and RER in CL-treated mice with body mass as covariate. N=6,5. *, $p<0.05$, **, $p<0.01$

SUPPLEMENTAL FIGURE LEGENDS

Figure S1. AdIL10Rα KO mice are protected against diet-induced obesity and show increased thermogenesis.

(A) Body mass and composition of 10 week-old chow-fed mice. (B) RER, locomotion and ambulatory activity of chow-fed 10-week-old IL10Rα F/F and AdIL10Rα KO mice analyzed by Columbus Oxymax metabolic chambers (12 h light/dark cycles, 72 hr total duration, each light/dark bar represents 12 h duration; N = 9,7). (C) Body weight of mice fed chow diet for 10 weeks and then 60% high-fat diet (HFD) for 9 weeks. N = 7,5. (D) Pathway analysis (Gene Ontology, GO) from RNA-seq data in Figure 2C.

Figure S2. Enrichment of cells involved in lipid mobilization in Cluster 9 adipocytes.

(A and B) Gene set pathways obtained from GO Biological Processes and KEGG were used to find the functions of the different cell types. The top 5 enriched pathways determined by FDR from each cell type cluster were selected (from Table S1) and only unique pathways were kept (some top enriched pathways were shared across cell type clusters). Enriched pathways (rows) were clustered with hierarchical clustering. The size of each dot represents the -log10 FDR of the pathway enrichment and the color of each dot corresponds to the fold enrichment of each pathway (red- higher enrichment, grey- lower enrichment). Dotted blue squares highlight pathways enriched in cluster 9.

Figure S3. Type 9 cluster constitute of thermogenic adipocytes

(A) Normalized expression values of top adipocyte subtype-specific major clusters (1, 4, and 9) genes from Figure 4A plotted as violin plots with clusters as rows and expression levels of genes

as columns. (B) tSNE-plot showing cluster-specific expression of selected marker genes from aggregated tSNE-plot in Fig. 4A. Black arrow indicates Type 9 cluster. (C) Normalized expression values of indicated genes plotted as violin plots with clusters as rows and expression levels of genes as columns.

Figure S4. Thermogenic pathway is enriched in the Type 9 cluster of IL10Rα-deficient adipocytes.

(A) Heatmap showing fold enrichment of pathways abundant in the adipocytes of AdIL10Rα KO mice compared to controls. DEG analysis of N represent Adipq-CRE Negative IL10RαF/F (IL10RαF/F) and P represent Adipoq-Cre Positive (AdIL10Rα KO) mice was performed and fold-change was calculated as Log2FC(N/P) and gene ontology analysis was performed for genes enriched in P over N and plotted as a heatmap as fold-enrichment (0 to >10) and $p<0.001$. Shades of blue indicate highly enriched pathway in P with fold-enrichment >10. (B) Violin plot showing expression levels of indicated genes in iWAT adipocytes of AdIL10Rα KO mice and controls from SNAP-seq data (Fig. 4)

REFERENCES

Bachman, E.S., Dhillon, H., Zhang, C.Y., Cinti, S., Bianco, A.C., Kobilka, B.K., and Lowell, B.B. (2002). betaAR signaling required for diet-induced thermogenesis and obesity resistance. Science *297*, 843-845.

Bapat, S.P., Myoung Suh, J., Fang, S., Liu, S., Zhang, Y., Cheng, A., Zhou, C., Liang, Y., LeBlanc, M., Liddle, C., et al. (2015). Depletion of fat-resident Treg cells prevents age-associated insulin resistance. Nature *528*, 137-141.

Bartness, T.J., Liu, Y., Shrestha, Y.B., and Ryu, V. (2014). Neural innervation of white adipose tissue and the control of lipolysis. Front Neuroendocrinol *35*, 473-493.

Benjamini, Y., and Hochberg, Y. (1995). Controlling the False Discovery Rate: A Practical and Powerful Approach to Multiple Testing. Journal of the Royal Statistical Society. Series B (Methodological) *57*, 289-300.

Blondel, V.D., Guillaume, J.-L., Lambiotte, R., and Lefebvre, E. (2008). Fast unfolding of communities in large networks. Journal of Statistical Mechanics: Theory and Experiment *2008*, P10008.

Bosma, M., Schuler, W., and Bosma, G. (1988). The scid mouse mutant. Curr Top Microbiol Immunol *137*, 197-202.

Burl, R.B., Ramseyer, V.D., Rondini, E.A., Pique-Regi, R., Lee, Y.-H., and Granneman, J.G. (2018). Deconstructing Adipogenesis Induced by β3-Adrenergic Receptor Activation with Single-Cell Expression Profiling. Cell Metabolism *28*, 300-309.e304.

Camell, C.D., Sander, J., Spadaro, O., Lee, A., Nguyen, K.Y., Wing, A., Goldberg, E.L., Youm, Y.H., Brown, C.W., Elsworth, J., et al. (2017). Inflammasome-driven catecholamine catabolism in macrophages blunts lipolysis during ageing. Nature *550*, 119-123.

Cannon, B., and Nedergaard, J. (2004). Brown adipose tissue: function and physiological significance. Physiol Rev *84*, 277-359.

Carter, S., Miard, S., Caron, A., Salle-Lefort, S., St-Pierre, P., Anhe, F.F., Lavoie-Charland, E., Blais-Lecours, P., Drolet, M.C., Lefebvre, J.S., et al. (2018). Loss of OcaB Prevents Age-Induced Fat Accretion and Insulin Resistance by Altering B-Lymphocyte Transition and Promoting Energy Expenditure. Diabetes *67*, 1285-1296.

Chechi, K., Carpentier, A.C., and Richard, D. (2013). Understanding the brown adipocyte as a contributor to energy homeostasis. Trends Endocrinol Metab *24*, 408-420.

Chen, J., Cheung, F., Shi, R., Zhou, H., Lu, W., Candia, J., Kotliarov, Y., Stagliano, K.R., Tsang, J.S., and Consortium, C. (2018). PBMC fixation and processing for Chromium single-cell RNA sequencing. Journal of Translational Medicine *16*, 198.

Cohen, P., Levy, J.D., Zhang, Y., Frontini, A., Kolodin, D.P., Svensson, K.J., Lo, J.C., Zeng, X., Ye, L., Khandekar, M.J., et al. (2014). Ablation of PRDM16 and beige adipose causes metabolic dysfunction and a subcutaneous to visceral fat switch. Cell *156*, 304-316.

Duncan, R.E., Ahmadian, M., Jaworski, K., Sarkadi-Nagy, E., and Sul, H.S. (2007). Regulation of lipolysis in adipocytes. Annu Rev Nutr *27*, 79-101.

Hagberg, C.E., Li, Q., Kutschke, M., Bhowmick, D., Kiss, E., Shabalina, I.G., Harms, M.J., Shilkova, O., Kozina, V., Nedergaard, J., et al. (2018). Flow Cytometry of Mouse and Human Adipocytes for the Analysis of Browning and Cellular Heterogeneity. Cell Rep *24*, 2746-2756 e2745.

Han, X., Wang, R., Zhou, Y., Fei, L., Sun, H., Lai, S., Saadatpour, A., Zhou, Z., Chen, H., Ye, F., et al. (2018). Mapping the Mouse Cell Atlas by Microwell-Seq. Cell *172*, 1091-1107.e1017.

Harms, M., and Seale, P. (2013). Brown and beige fat: development, function and therapeutic potential. Nat Med *19*, 1252-1263.

Hepler, C., Shan, B., Zhang, Q., Henry, G.H., Shao, M., Vishvanath, L., Ghaben, A.L., Mobley, A.B., Strand, D., Hon, G.C., et al. (2018). Identification of functionally distinct fibro-inflammatory and adipogenic stromal subpopulations in visceral adipose tissue of adult mice. eLife *7*, e39636.

Jaworski, K., Sarkadi-Nagy, E., Duncan, R.E., Ahmadian, M., and Sul, H.S. (2007). Regulation of triglyceride metabolism. IV. Hormonal regulation of lipolysis in adipose tissue. Am J Physiol Gastrointest Liver Physiol *293*, G1-4.

Laurens van der Maaten, G.H. (2008). Visualizing Data using t-SNE. Journal of Machine Learning Research *9*, 2579-2605.

Lee, K.Y., Luong, Q., Sharma, R., Dreyfuss, J.M., Ussar, S., and Kahn, C.R. (2019). Developmental and functional heterogeneity of white adipocytes within a single fat depot. EMBO J *38*.

Lun, A.T.L., Riesenfeld, S., Andrews, T., Dao, T.P., Gomes, T., Marioni, J.C., and Jamboree, p.i.t.s.H.C.A. (2019). EmptyDrops: distinguishing cells from empty droplets in droplet-based single-cell RNA sequencing data. Genome Biology *20*, 63.

Mina, A.I., LeClair, R.A., LeClair, K.B., Cohen, D.E., Lantier, L., and Banks, A.S. (2018). CalR: A Web-Based Analysis Tool for Indirect Calorimetry Experiments. Cell Metab *28*, 656-666 e651.

Patsouris, D., Qi, P., Abdullahi, A., Stanojcic, M., Chen, P., Parousis, A., Amini-Nik, S., and Jeschke, M.G. (2015). Burn Induces Browning of the Subcutaneous White Adipose Tissue in Mice and Humans. Cell Rep *13*, 1538-1544.

Petruzzelli, M., Schweiger, M., Schreiber, R., Campos-Olivas, R., Tsoli, M., Allen, J., Swarbrick, M., Rose-John, S., Rincon, M., Robertson, G., et al. (2014). A switch from white to brown fat increases energy expenditure in cancer-associated cachexia. Cell Metab *20*, 433-447.

Petukhov, V., Guo, J., Baryawno, N., Severe, N., Scadden, D.T., Samsonova, M.G., and Kharchenko, P.V. (2018). dropEst: pipeline for accurate estimation of molecular counts in droplet-based single-cell RNA-seq experiments. Genome Biol *19*, 78.

Pirzgalska, R.M., Seixas, E., Seidman, J.S., Link, V.M., Sanchez, N.M., Mahu, I., Mendes, R., Gres, V., Kubasova, N., Morris, I., et al. (2017). Sympathetic neuron-associated macrophages contribute to obesity by importing and metabolizing norepinephrine. Nat Med *23*, 1309-1318.

Rajbhandari, P., Thomas, B.J., Feng, A.C., Hong, C., Wang, J., Vergnes, L., Sallam, T., Wang, B., Sandhu, J., Seldin, M.M., et al. (2018). IL-10 Signaling Remodels Adipose Chromatin Architecture to Limit Thermogenesis and Energy Expenditure. Cell *172*, 218-233 e217.

Rogers, G.W., Brand, M.D., Petrosyan, S., Ashok, D., Elorza, A.A., Ferrick, D.A., and Murphy, A.N. (2011). High throughput microplate respiratory measurements using minimal quantities of isolated mitochondria. PLoS One *6*, e21746.

Rosen, E.D., and Spiegelman, B.M. (2014). What we talk about when we talk about fat. Cell *156*, 20-44.

Saely, C.H., Geiger, K., and Drexel, H. (2012). Brown versus white adipose tissue: a mini-review. Gerontology *58*, 15-23.

Saraiva, M., and O'Garra, A. (2010). The regulation of IL-10 production by immune cells. Nat Rev Immunol *10*, 170-181.

Schaffler, A., and Scholmerich, J. (2010). Innate immunity and adipose tissue biology. Trends Immunol *31*, 228-235.

Schaum, N., Karkanias, J., Neff, N.F., May, A.P., Quake, S.R., Wyss-Coray, T., Darmanis, S., Batson, J., Botvinnik, O., Chen, M.B., et al. (2018). Single-cell transcriptomics of 20 mouse organs creates a Tabula Muris. Nature *562*, 367-372.

Schreiber, R., Diwoky, C., Schoiswohl, G., Feiler, U., Wongsiriroj, N., Abdellatif, M., Kolb, D., Hoeks, J., Kershaw, E.E., Sedej, S., et al. (2017). Cold-Induced Thermogenesis Depends on ATGL-Mediated Lipolysis in Cardiac Muscle, but Not Brown Adipose Tissue. Cell Metab *26*, 753-763 e757.

Sell, H., Habich, C., and Eckel, J. (2012). Adaptive immunity in obesity and insulin resistance. Nat Rev Endocrinol *8*, 709-716.

Song, N.-J., Choi, S., Rajbhandari, P., Chang, S.-H., Kim, S., Vergnes, L., Kwon, S.-M., Yoon, J.-H., Lee, S., Ku, J.-M., et al. (2016). Prdm4 induction by the small molecule butein promotes white adipose tissue browning. Nat Chem Biol *advance online publication*.

Song, W., Luo, Q., Zhang, Y., Zhou, L., Liu, Y., Ma, Z., Guo, J., Huang, Y., Cheng, L., Meng, Z., et al. (2019). Organic cation transporter 3 (Oct3) is a distinct catecholamines clearance route in adipocytes mediating the beiging of white adipose tissue. PLoS Biol *17*, e2006571.

Stoeckius, M., Hafemeister, C., Stephenson, W., Houck-Loomis, B., Chattopadhyay, P.K., Swerdlow, H., Satija, R., and Smibert, P. (2017). Simultaneous epitope and transcriptome measurement in single cells. Nature Methods *14*, 865.

Takahashi, A., Adachi, S., Morita, M., Tokumasu, M., Natsume, T., Suzuki, T., and Yamamoto, T. (2015). Post-transcriptional Stabilization of Ucp1 mRNA Protects Mice from Diet-Induced Obesity. Cell Rep *13*, 2756-2767.

Tong, A.J., Liu, X., Thomas, B.J., Lissner, M.M., Baker, M.R., Senagolage, M.D., Allred, A.L., Barish, G.D., and Smale, S.T. (2016). A Stringent Systems Approach Uncovers Gene-Specific Mechanisms Regulating Inflammation. Cell *165*, 165-179.

Villanueva, C.J., Vergnes, L., Wang, J., Drew, B.G., Hong, C., Tu, Y., Hu, Y., Peng, X., Xu, F., Saez, E., et al. (2013). Adipose subtype-selective recruitment of TLE3 or Prdm16 by PPARgamma specifies lipid storage versus thermogenic gene programs. Cell Metab *17*, 423-435.

Vitali, A., Murano, I., Zingaretti, M.C., Frontini, A., Ricquier, D., and Cinti, S. (2012). The adipose organ of obesity-prone C57BL/6J mice is composed of mixed white and brown adipocytes. J Lipid Res *53*, 619-629.

Wajchenberg, B.L. (2000). Subcutaneous and visceral adipose tissue: their relation to the metabolic syndrome. Endocr Rev *21*, 697-738.

Wang, Q.A., Tao, C., Gupta, R.K., and Scherer, P.E. (2013). Tracking adipogenesis during white adipose tissue development, expansion and regeneration. Nat Med *19*, 1338-1344.

Wernstedt Asterholm, I., Tao, C., Morley, T.S., Wang, Q.A., Delgado-Lopez, F., Wang, Z.V., and Scherer, P.E. (2014). Adipocyte inflammation is essential for healthy adipose tissue expansion and remodeling. Cell Metab *20*, 103-118.

Zechner, R., Kienesberger, P.C., Haemmerle, G., Zimmermann, R., and Lass, A. (2009). Adipose triglyceride lipase and the lipolytic catabolism of cellular fat stores. J Lipid Res *50*, 3-21.

Zhang, X., Lan, Y., Xu, J., Quan, F., Zhao, E., Deng, C., Luo, T., Xu, L., Liao, G., Yan, M., et al. (2018). CellMarker: a manually curated resource of cell markers in human and mouse. Nucleic Acids Research *47*, D721-D728.

Zywitza, V., Misios, A., Bunatyan, L., Willnow, T.E., and Rajewsky, N. (2018). Single-Cell Transcriptomics Characterizes Cell Types in the Subventricular Zone and Uncovers Molecular Defects Impairing Adult Neurogenesis. Cell Reports *25*, 2457-2469.e2458.

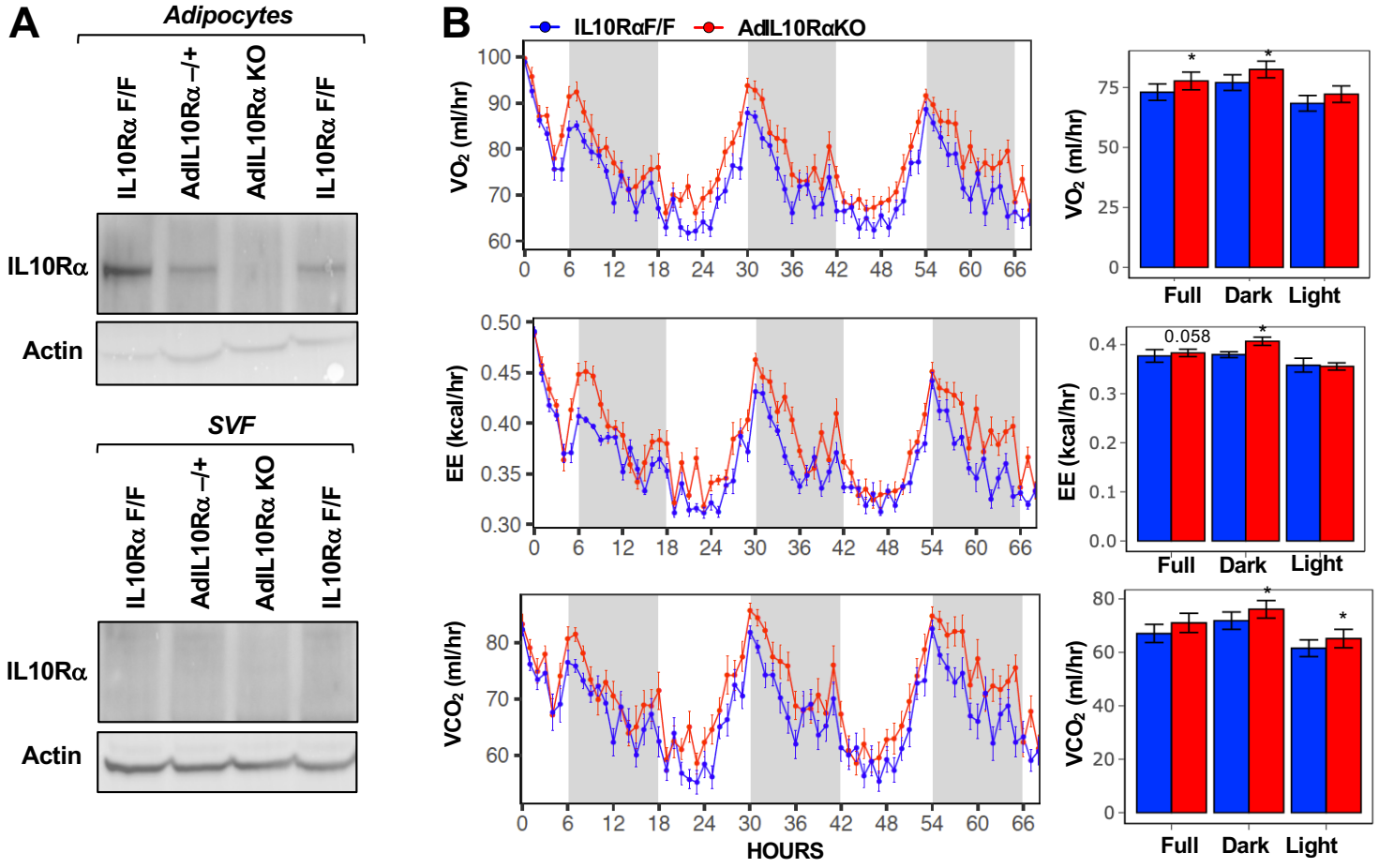

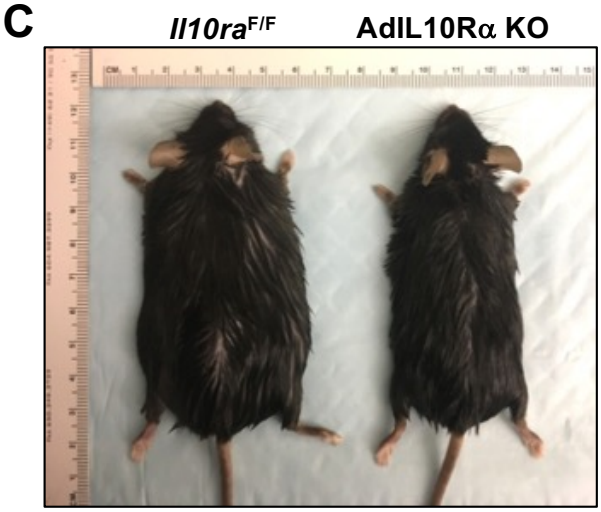

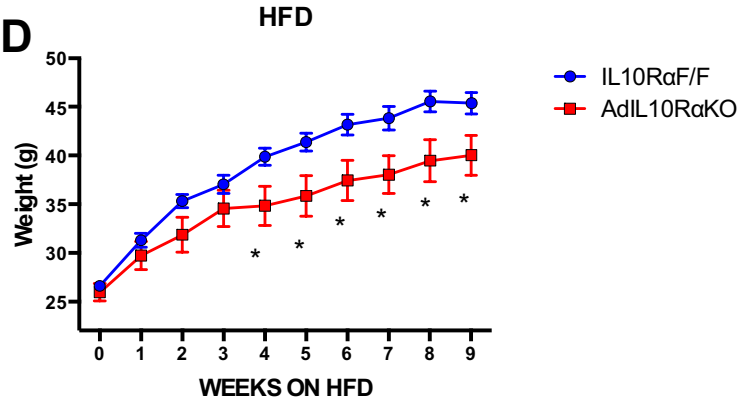

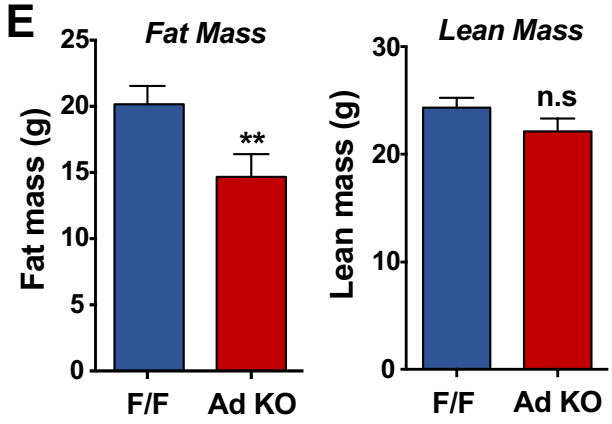

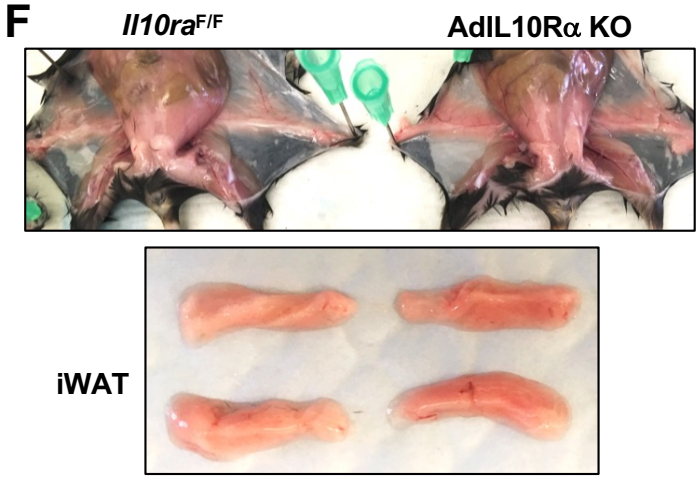

Rajbhandari Fig 1

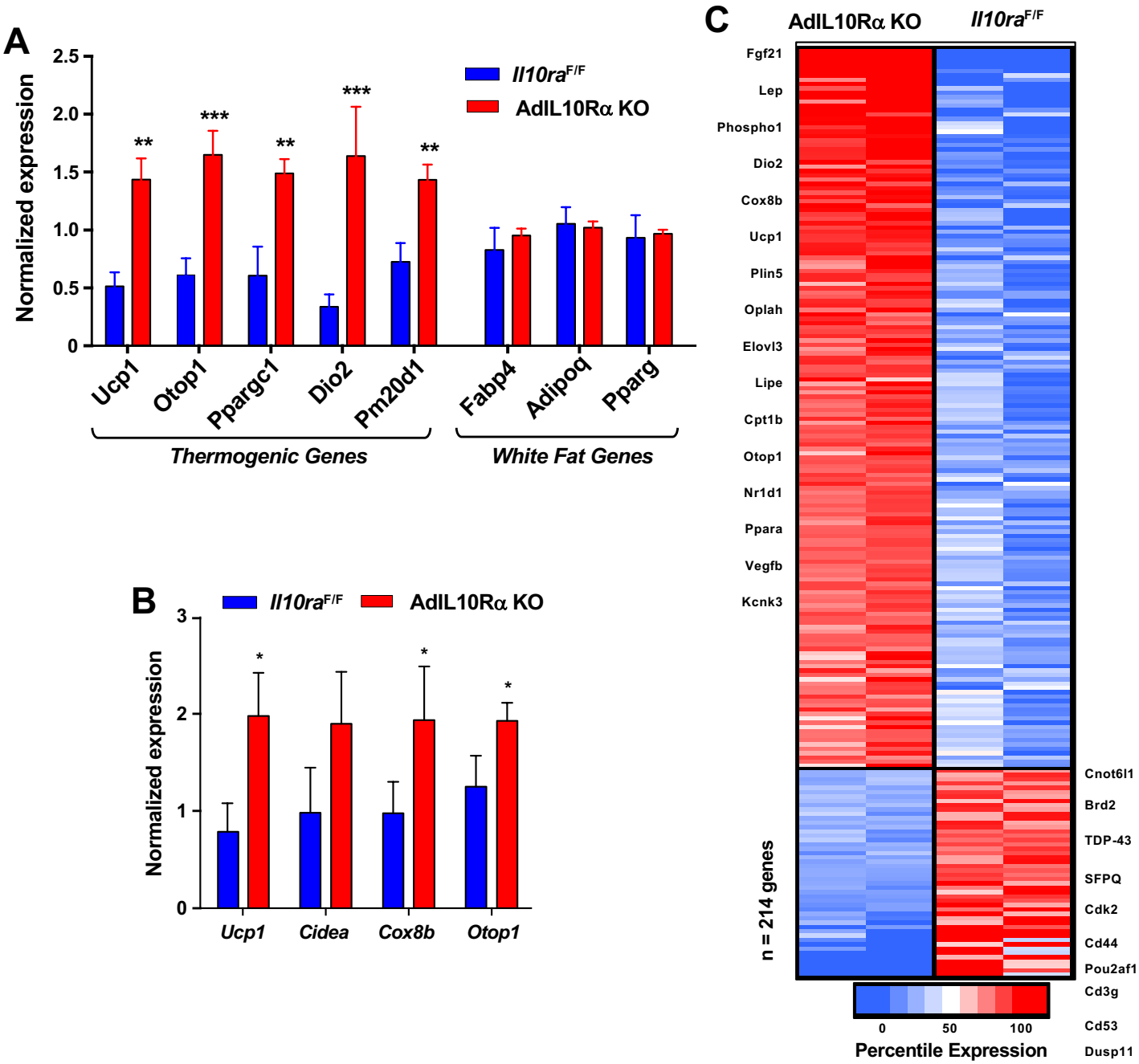

Rajbhandari Fig 2

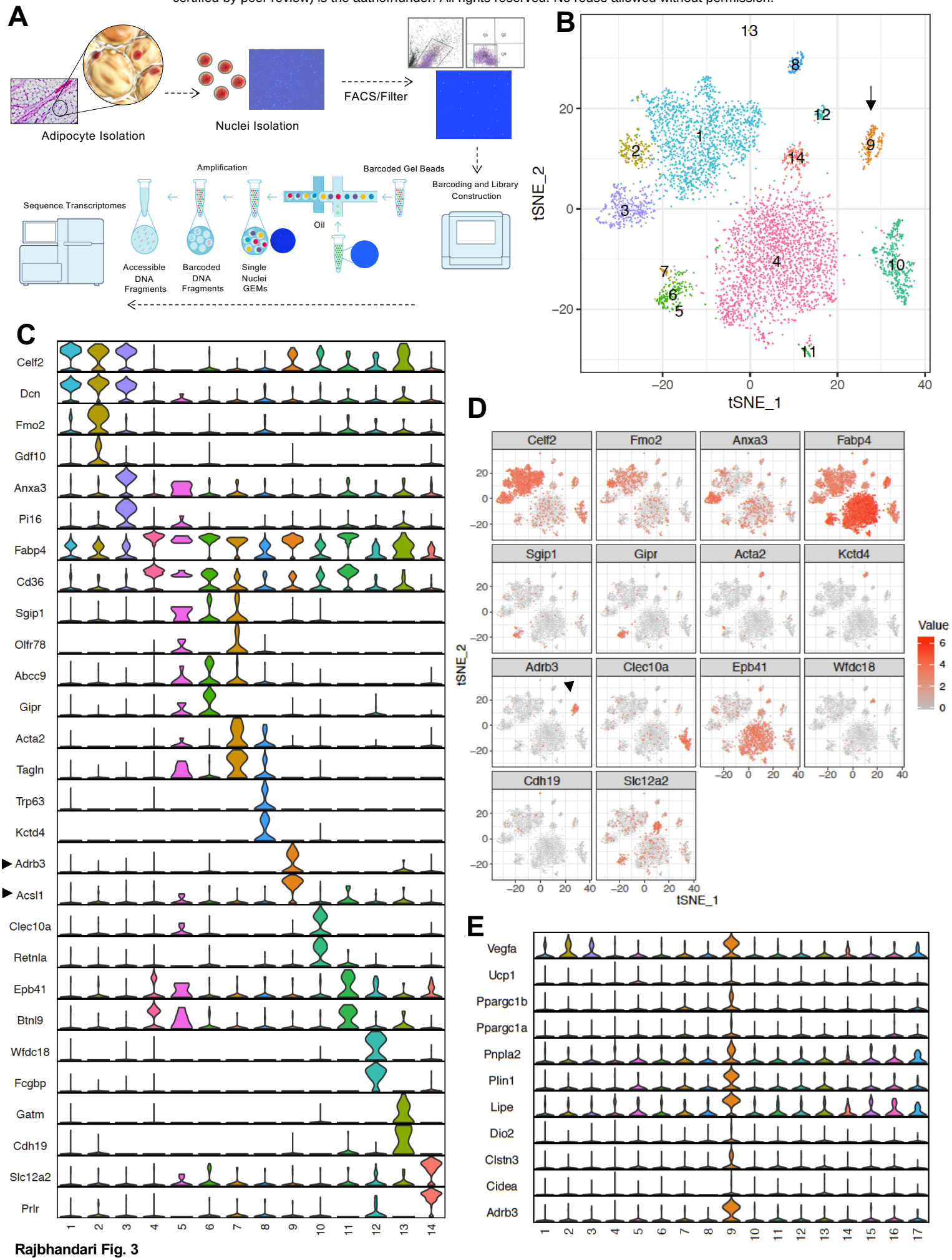

Rajbhandari Fig. 3

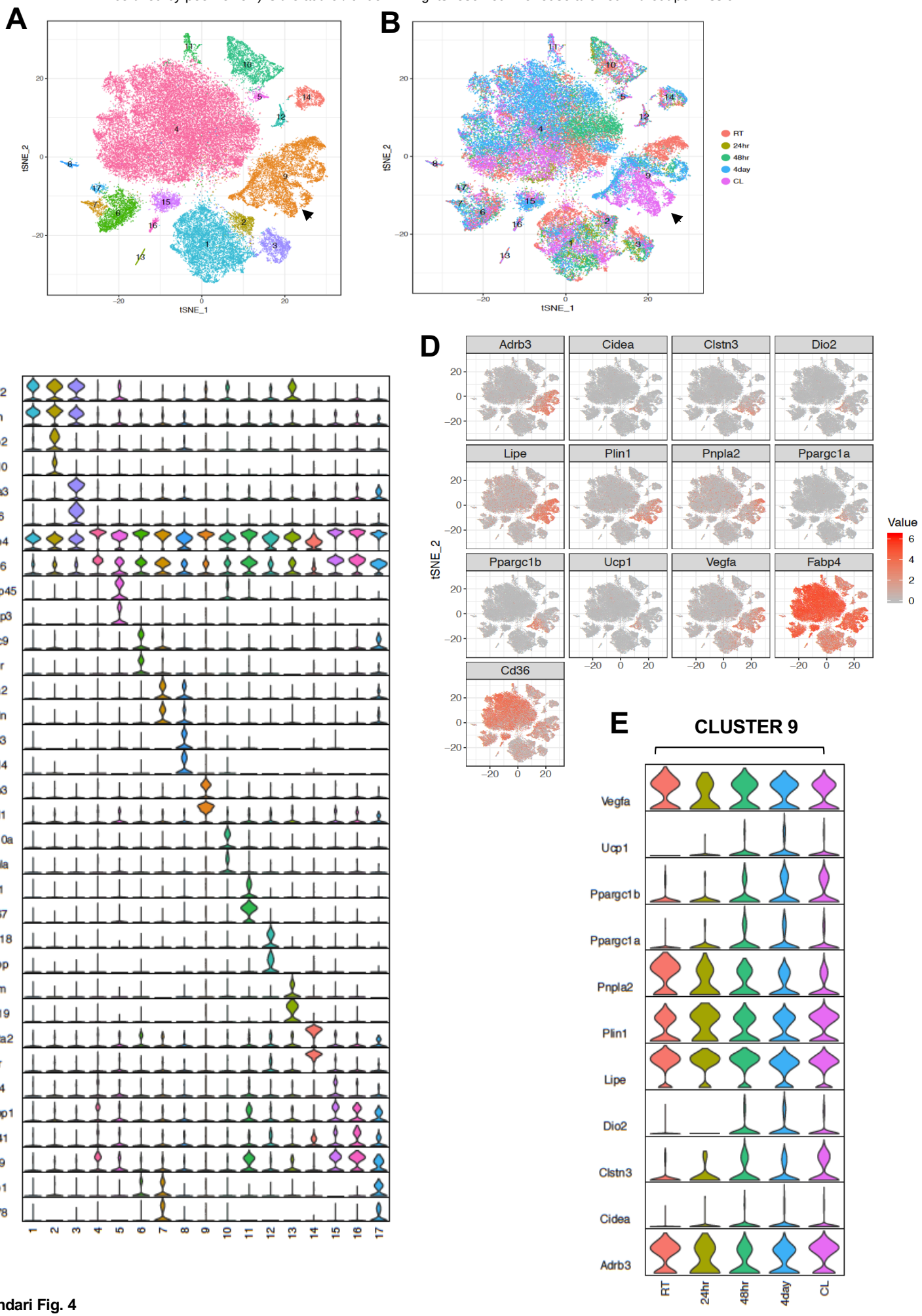

Rajbhandari Fig. 4

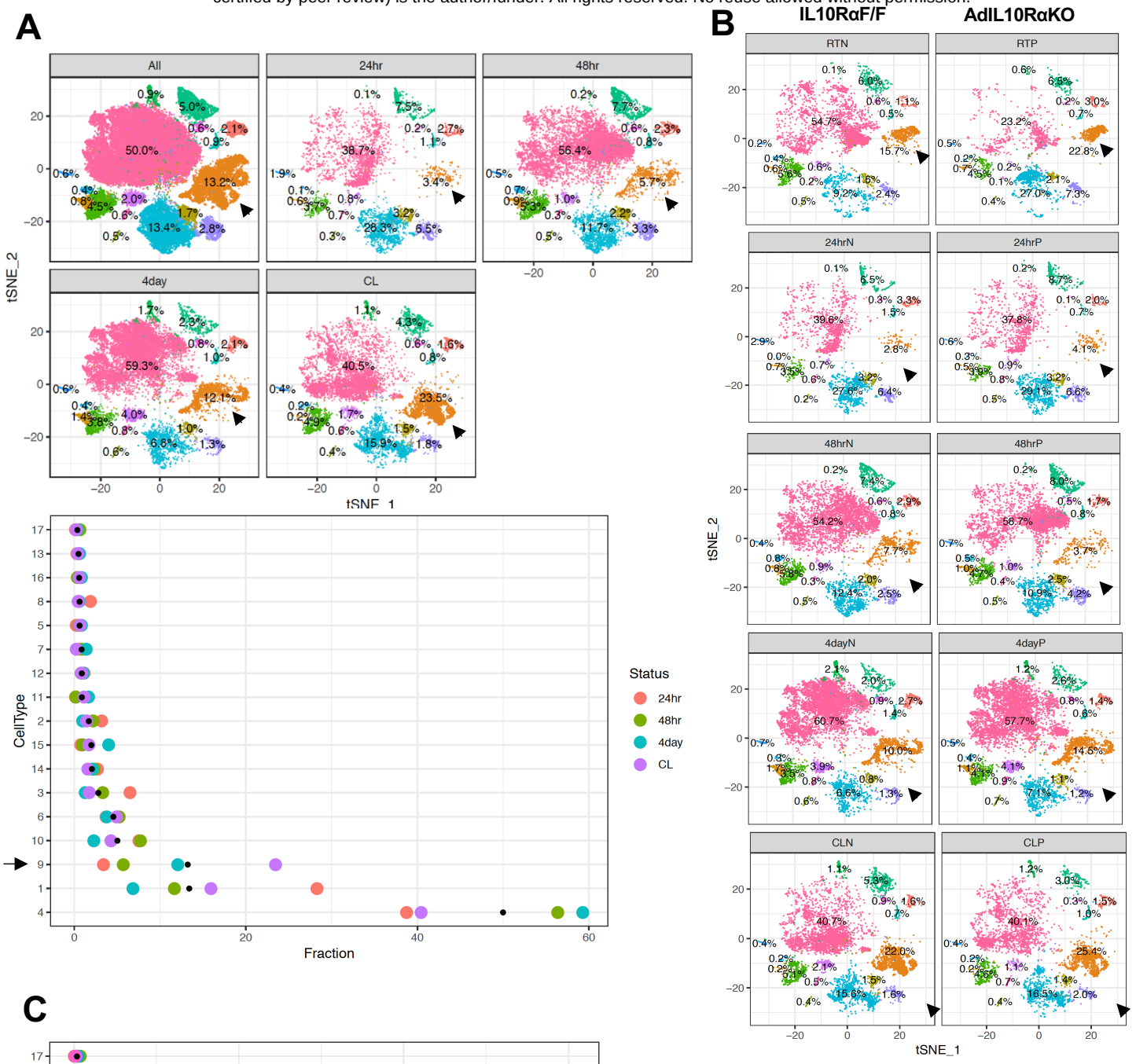

Rajbhandari Fig. 5

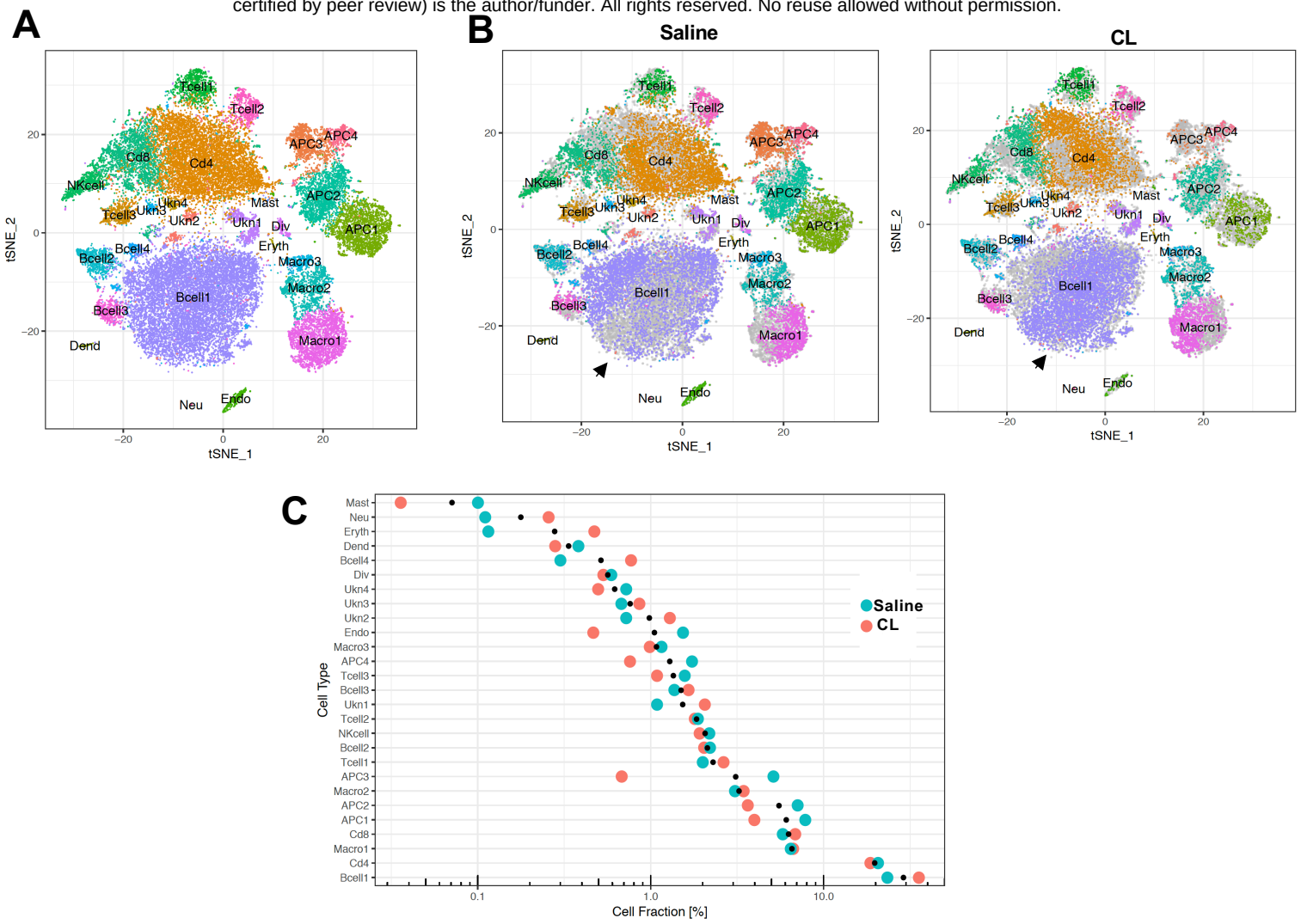

Rajbhandari Fig. 6

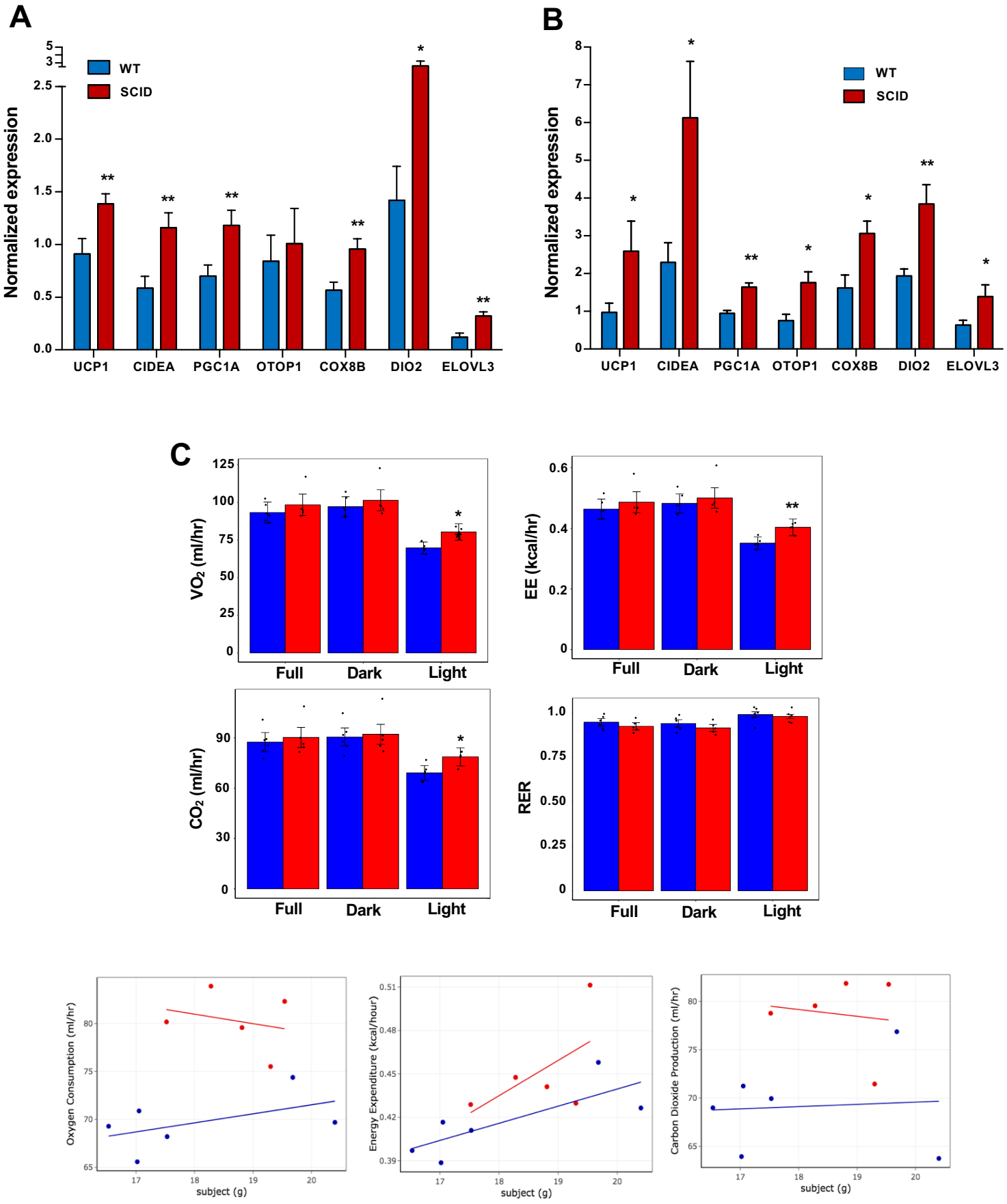

Rajbhandari Fig. 7

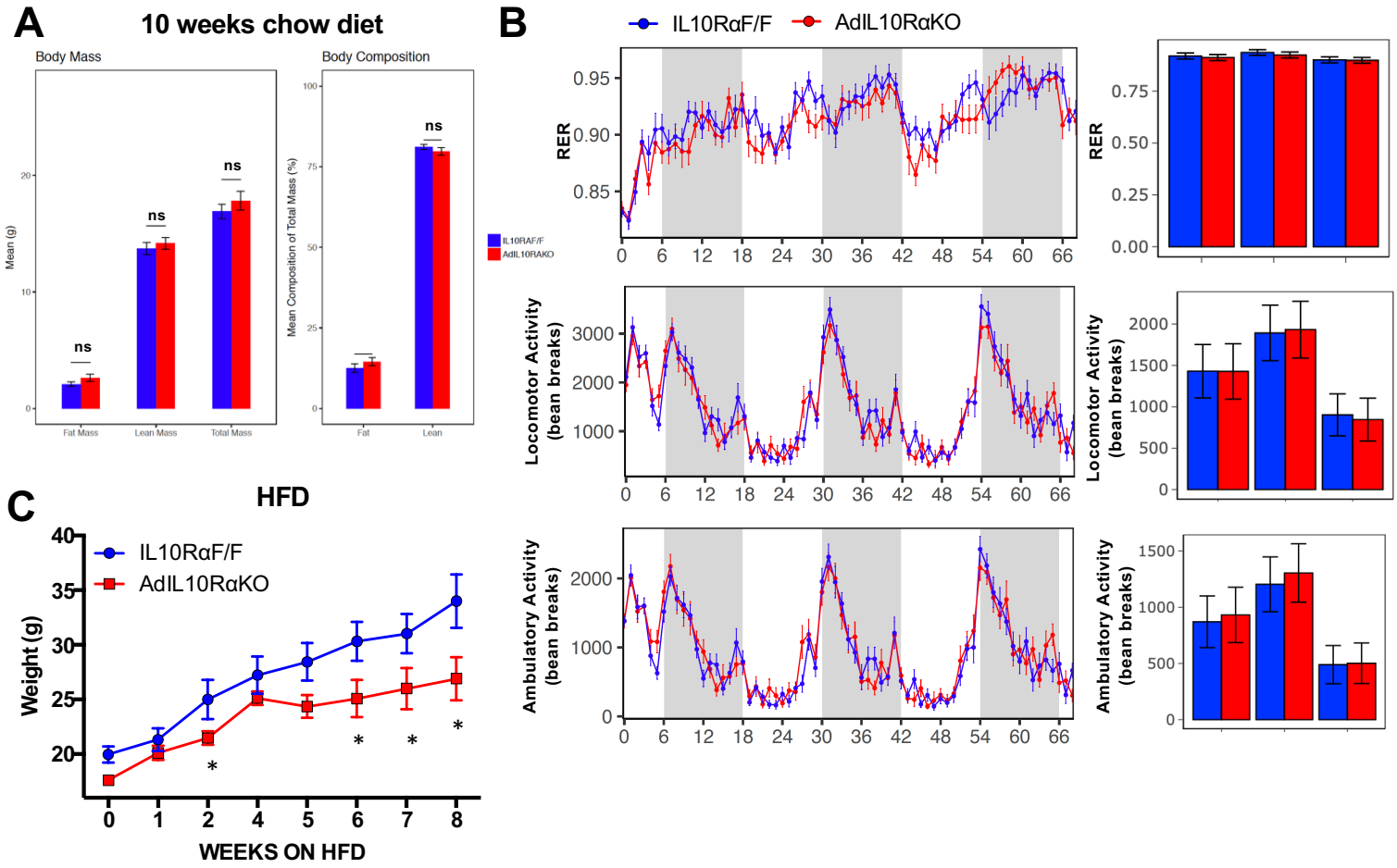

D

GO biological process complete	# in Mouse Genome	# in Input Gene List	# Genes Expected	Fold Enrichment	P value
positive regulation of lipid biosynthetic process	92	8	0.66	12.18	4.93E-03
--> positive regulation of lipid metabolic process	153	11	1.09	10.07	2.24E-04
--> positive regulation of biological process	5893	70	42.09	1.66	1.81E-02
--> regulation of metabolic process	5649	69	40.35	1.71	7.84E-03
--> regulation of lipid metabolic process	328	14	2.34	5.98	1.40E-03
--> regulation of lipid biosynthetic process	167	11	1.19	9.22	5.20E-04
positive regulation of cold-induced thermogenesis	95	8	0.68	11.79	6.19E-03
--> regulation of cold-induced thermogenesis	141	9	1.01	8.94	1.10E-02
regulation of lipid transport	112	8	0.8	10	1.98E-02
--> regulation of lipid localization	142	10	1.01	9.86	1.18E-03
lipid localization	278	12	1.99	6.04	9.87E-03
lipid metabolic process	1045	26	7.46	3.48	3.21E-04
--> metabolic process	7138	79	50.98	1.55	4.30E-02
regulation of apoptotic process	1468	31	10.48	2.96	5.20E-04
--> regulation of programmed cell death	1488	31	10.63	2.92	7.01E-04
--> regulation of cell death	1636	35	11.68	3	4.33E-05
regulation of catalytic activity	1793	32	12.81	2.5	1.24E-02
regulation of signal transduction	2704	45	19.31	2.33	5.28E-04
--> regulation of cell communication	3110	51	22.21	2.3	5.51E-05
--> regulation of signaling	3125	51	22.32	2.29	6.28E-05
--> regulation of response to stimulus	3795	54	27.1	1.99	2.09E-03
negative regulation of cellular process	4443	57	31.73	1.8	2.98E-02
--> negative regulation of biological process	4959	61	35.42	1.72	4.62E-02
Unclassified	1822	3	13.01	0.23	0.00E+00

	# in Mouse Genome	# in Input Gene List	# Genes Expected	Fold Enrichment	P value
adaptive immune response	468	9	0.97	9.31	4.07E-03
Unclassified	1822	3	3.76	0.8	0.00E+00

Rajbhandari Fig. S1

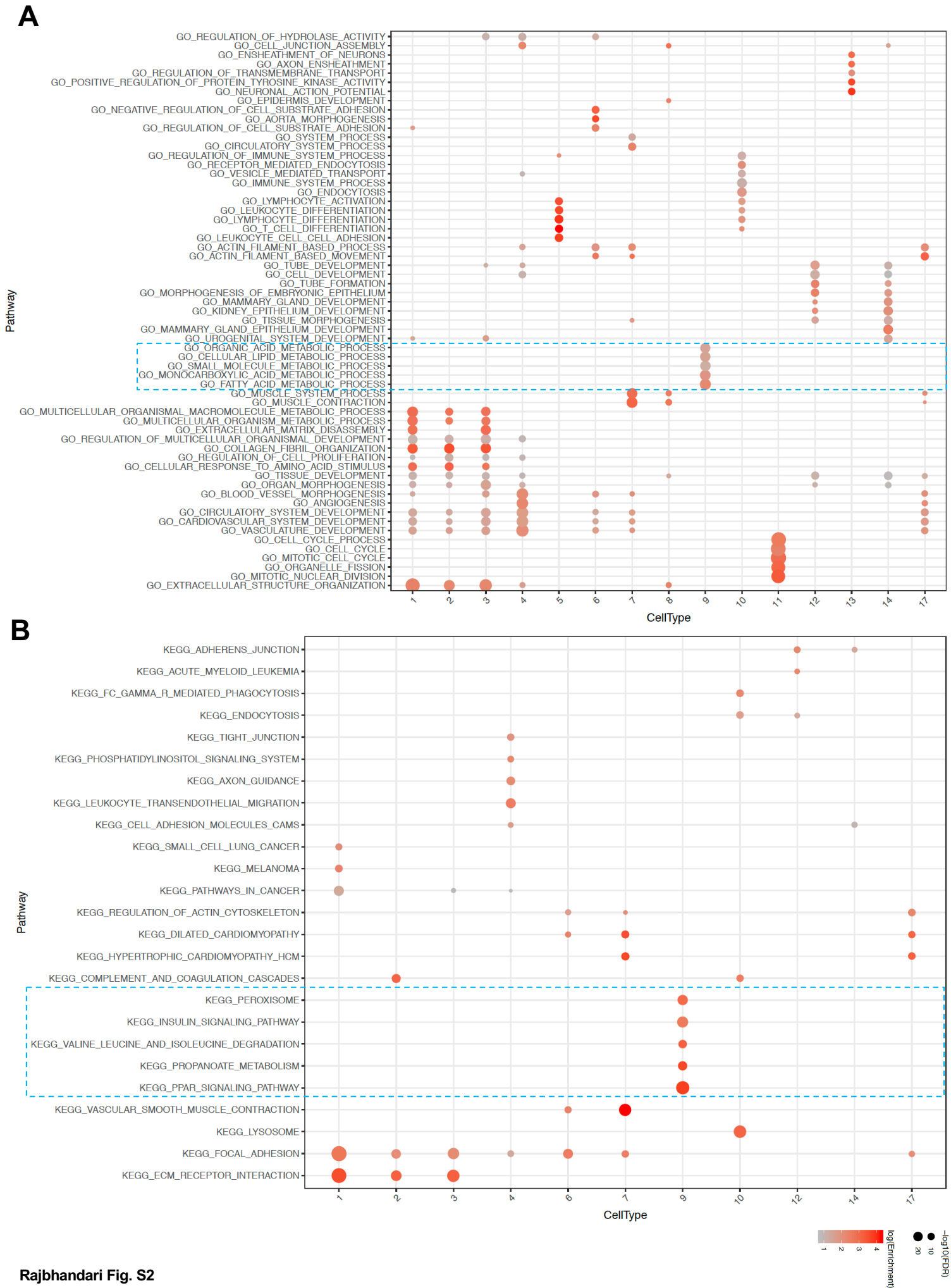

Rajbhandari Fig. S2

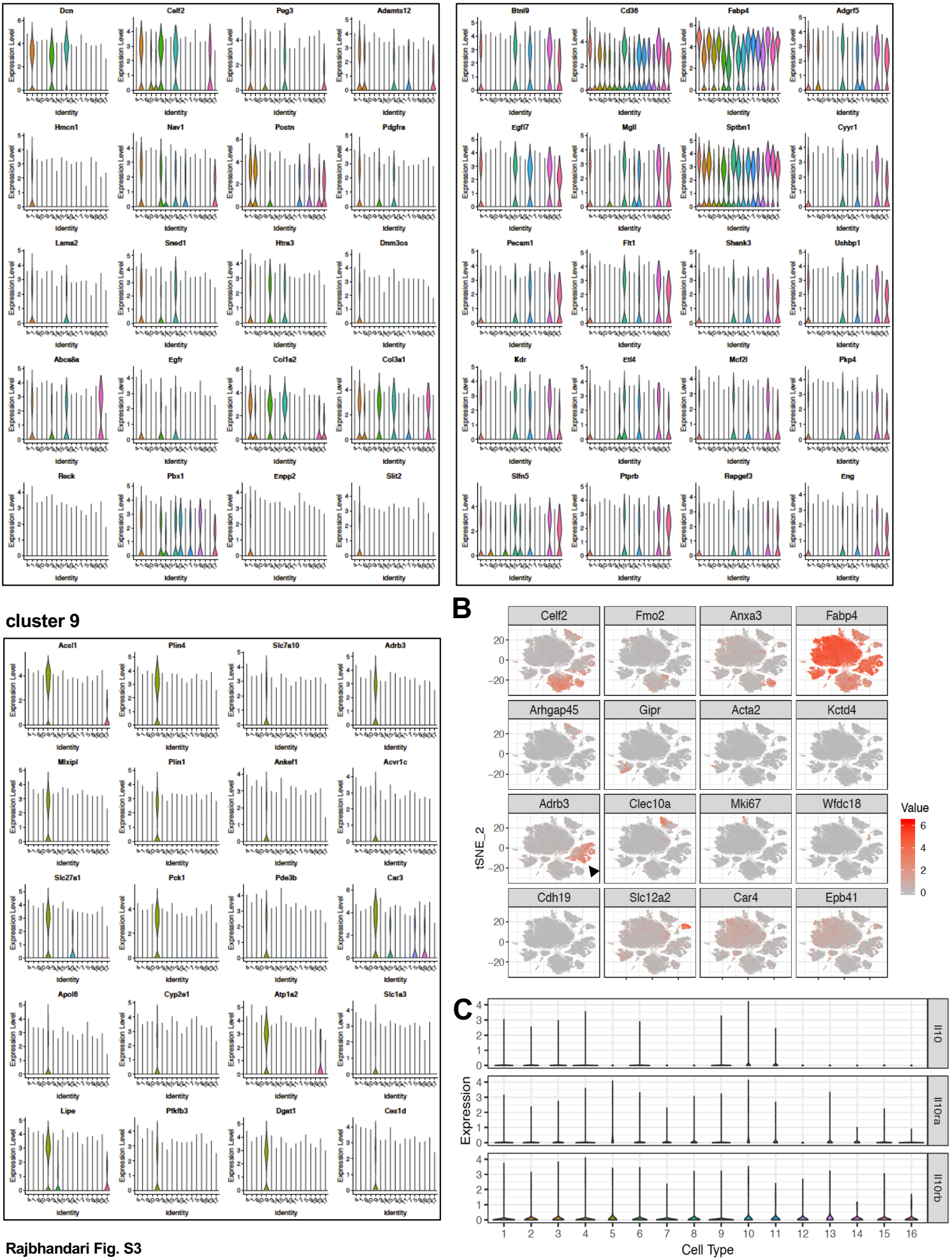

Rajbhandari Fig. S3

A

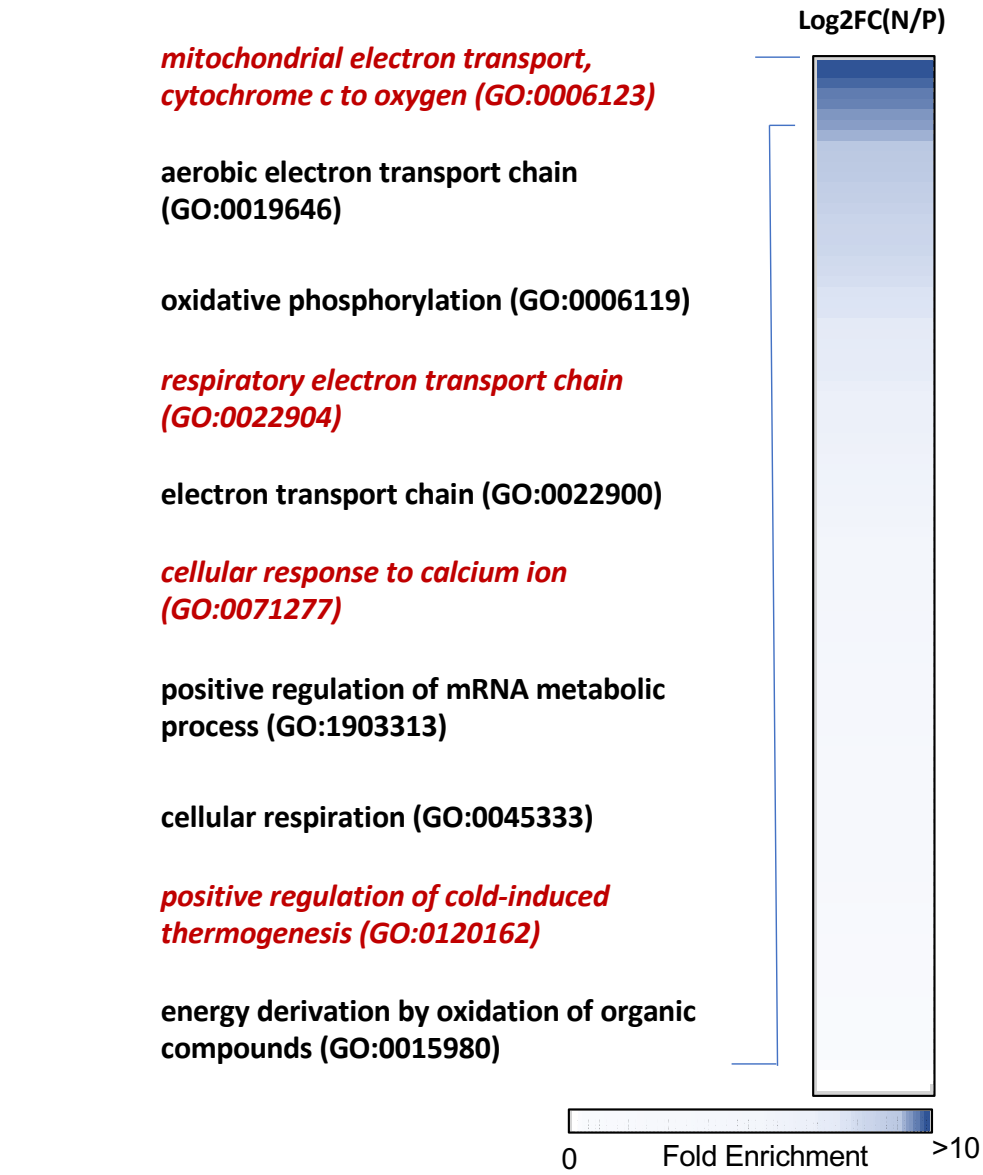

B

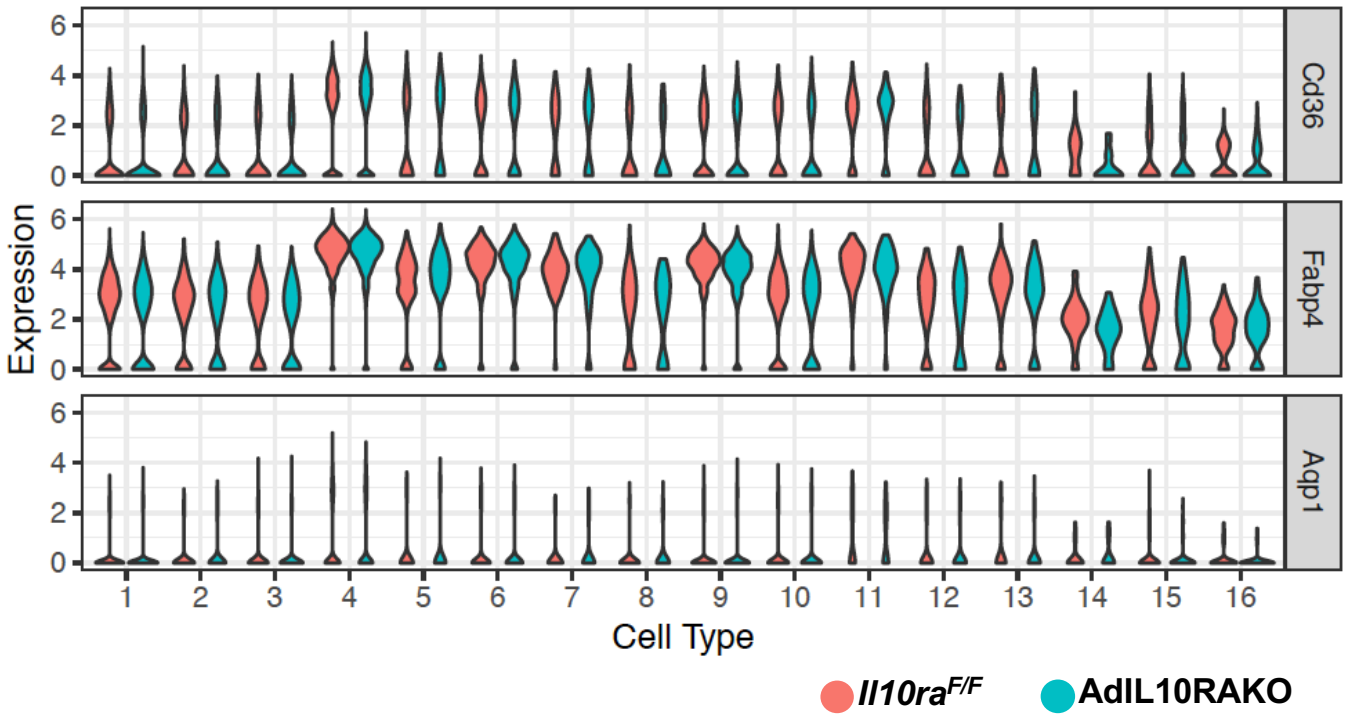

Rajbhandari Fig. S4